



## OPEN ACCESS

## EDITED BY

Elizabeth Christ Sklute,  
Los Alamos National Laboratory (DOE),  
United States

## REVIEWED BY

Akos Kereszturi,  
Hungarian Academy of Sciences  
(MTA), Hungary  
Jeff Johnson,  
Johns Hopkins University, United States  
Kevin Robertson,  
Brown University, United States

## \*CORRESPONDENCE

Rachel Y. Sheppard,  
✉ rsheppard@psi.edu

RECEIVED 20 December 2024

ACCEPTED 31 March 2025

PUBLISHED 28 April 2025

## CITATION

Sheppard RY, Loizeau D, Fraeman AA,  
Rampe EB, Pilorget C and Bibring J-P (2025)  
Mg-sulfate can spectrally obscure siderite:  
implications for martian surface carbonates.  
*Front. Astron. Space Sci.* 12:1549242.  
doi: 10.3389/fspas.2025.1549242

## COPYRIGHT

© 2025 Sheppard, Loizeau, Fraeman, Rampe,  
Pilorget and Bibring. This is an open-access  
article distributed under the terms of the  
[Creative Commons Attribution License \(CC  
BY\)](https://creativecommons.org/licenses/by/4.0/). The use, distribution or reproduction in  
other forums is permitted, provided the  
original author(s) and the copyright owner(s)  
are credited and that the original publication  
in this journal is cited, in accordance with  
accepted academic practice. No use,  
distribution or reproduction is permitted  
which does not comply with these terms.

# Mg-sulfate can spectrally obscure siderite: implications for martian surface carbonates

Rachel Y. Sheppard<sup>1,2\*</sup>, Damien Loizeau<sup>1</sup>, Abigail A. Fraeman<sup>3</sup>,  
Elizabeth B. Rampe<sup>4</sup>, Cédric Pilorget<sup>1,5</sup> and Jean-Pierre Bibring<sup>1</sup>

<sup>1</sup>Institut d'Astrophysique Spatiale, Université Paris-Saclay, CNRS, Orsay, France, <sup>2</sup>Planetary Science Institute, Tucson, AZ, United States, <sup>3</sup>Jet Propulsion Laboratory, California Institute of Technology, Pasadena, CA, United States, <sup>4</sup>Astromaterials Research and Exploration Science Division, NASA Johnson Space Center, Houston, TX, United States, <sup>5</sup>Institut Universitaire de France, Paris, France

**Introduction:** The search for carbonates on the martian surface has been ongoing since the Viking missions. Recently the Curiosity rover observed carbonate *in situ* in Gale crater, however it is not visible from orbit. This study investigates the role of Mg-sulfate, one of the most common secondary minerals on Mars, in obscuring the spectral signatures of carbonates in orbital datasets.

**Methods:** We collect spectral images of polyhydrated Mg-sulfate and siderite physical mixtures in various proportions exposed to a dry environmental chamber. We also collect spectral images at multiple timepoints to track the temporal evolution of the mixtures as the Mg-sulfate component dehydrates from 7H<sub>2</sub>O epsomite to 2H<sub>2</sub>O X-ray amorphous forms, particularly focusing on how sulfate dehydration impacts the visibility of carbonate absorption bands at 2.3 and 2.5 μm.

**Results:** Our results reveal that Mg-sulfate can obscure the carbonate signature, especially the 2.3 μm band.

**Discussion:** These findings suggest that Mg-sulfate deposits may mask carbonates from orbital spectrometers like CRISM and OMEGA, implying that carbonate could be present in more locations on Mars than current orbital observations indicate.

## KEYWORDS

Mars, carbonate, spectroscopy, MicrOmega, sulfate

## 1 Introduction

### 1.1 The paradox of martian carbonates

Carbonates most commonly precipitate from water, and their specific type (cation attached to the CO<sub>3</sub><sup>2-</sup> carbonate anion) is a valuable record that can constrain fluid composition, pH, and temperature. On Earth, atmospheric CO<sub>2</sub> dissolves into surface water, producing carbonic acid which increases the capacity of the water to dissolve minerals in contact with the water; the carbonic acid can then dissociate forming bicarbonate, which can combine with cations in the water to precipitate carbonates (e.g., Drever, 1997; Bridges et al., 2019). Thermodynamic modeling of ancient martian surface waters in contact with a CO<sub>2</sub>-rich atmosphere suggests that carbonates should

have formed in large quantities during the Noachian (Banin et al., 2007; Fairén et al., 2004; King and McSween, 2005), especially the Fe(II)-carbonate siderite which is the most insoluble major common carbonate and should precipitate first under early Mars conditions (Catling, 1999).

However, the field of remote sensing has noted for decades the dearth of orbital carbonate detections on Mars. Carbonates have distinct spectral features within the spectral ranges of the current generation of orbital spectrometers including CRISM and OMEGA (Changela et al., 2021). As such they have been detected by orbital spectrometers across the martian surface (Ehlmann et al., 2008; Ehlmann et al., 2009; Mustard et al., 2010; Niles et al., 2013; Bridges et al., 2019; Section 1.3 below), but rarely in as great abundance as theorized, possibly due to dust cover, spectral mixing, and instrumental limitations (Ehlmann et al., 2009; Wray et al., 2016).

It was first proposed that areally widespread stable or metastable carbonates formed on Mars, perhaps from an early dense atmosphere or gas-solid weathering (O'Connor, 1968; Gooding et al., 1992; Squyres and Kasting, 1994; Bell et al., 1996), but were either destroyed by acidic groundwaters and/or volcanic gases (Bell et al., 1996; Catling, 1999; Burns and Fisher, 1990; Fairén et al., 2004; King et al., 2004) or else were buried by sedimentary/aeolian processes or lavas, obscuring them from orbital spectroscopy which is only sensitive to the upper 10 s of micrometers of the surface (Squyres and Kasting, 1994; Bell et al., 1996). More recently, it has been proposed that Mars did not produce widespread carbonates, either due to acidic surface water, low atmospheric  $p\text{CO}_2$ , atmospheric escape, or aqueous processes occurring in the subsurface out of contact with the  $\text{CO}_2$ -rich atmosphere (Burns, 1993; Hurowitz et al., 2006; Chevrier et al., 2007; Ehlmann et al., 2011; Bristow et al., 2017; Tosca et al., 2018). The concept of early atmospheric escape is supported by the low atmospheric  $\text{N}_2/\text{CO}_2$  ratio which should be higher than observed if a thick atmosphere had lost  $\text{CO}_2$  to carbonates (Bibring and Erard, 2001; Bibring et al., 2005; Yoshida et al., 2020).

Despite the relative absence of carbonate detections in Gale crater from orbital spectroscopy, the Mars Science Laboratory *Curiosity* rover detected abundant siderite in the orbitally defined "Mg-sulfate unit" (Tutolo et al., 2025). Siderite was identified in abundances of up to ~10 wt.% of the crystalline component of the bulk sample with the CheMin X-ray diffractometer (Blake et al., 2012), along with minor amounts of starkeyite ( $\text{MgSO}_4 \cdot 4\text{H}_2\text{O}$ ) or kieserite ( $\text{MgSO}_4 \cdot \text{H}_2\text{O}$ ). The Mg-sulfate unit covers an area of many 10 s of square kilometers, and the combination of areal extent and high concentration of siderite should have enabled its detection via orbital short-wave infrared reflectance spectroscopy.

We sought to examine whether the strong short-wave infrared absorption features of Mg-sulfate, one of the most common secondary minerals on the martian surface, may be obscuring orbital evidence of carbonates on the martian surface. Although generally forming under different pH and redox conditions, multiple primary or diagenetic aqueous episodes with changing conditions can cause physical co-occurrence of these phases, as has been seen in parts of Gale crater. It is important therefore to examine the link between small-scale co-existence of these phases and their spectral signatures that would be observed from orbit. We collected spectral image cubes of crystalline and X-ray amorphous polyhydrated Mg-sulfate

TABLE 1 Mineral name, formula, and hydration state for minerals relevant to this work.

Mineral name	Chemical formula	Hydration state
Siderite	$\text{Fe(II)CO}_3$	Anhydrous
Ankerite	$\text{Ca(Fe(II),Mg,Mn)(CO}_3)_2$	Anhydrous
Magnesite	$\text{MgCO}_3$	Anhydrous
Dolomite	$\text{Ca,Mg(CO}_3)_2$	Anhydrous
Epsomite	$\text{MgSO}_4 \cdot 7\text{H}_2\text{O}$	Polyhydrated
Starkeyite	$\text{MgSO}_4 \cdot 4\text{H}_2\text{O}$	Polyhydrated
Amorphous Mg-sulfate	$\text{MgSO}_4 \cdot n\text{H}_2\text{O}$	Polyhydrated
Kieserite	$\text{MgSO}_4 \cdot 1\text{H}_2\text{O}$	Monohydrated

and siderite, mixed at different ratios. Spectra were collected over the course of a month as the hydration state and crystallinity of Mg-sulfate evolved in exposure to the dry interior of the used environmental chamber.

## 1.2 Spectral features of sulfate and carbonate

Relevant minerals are listed in Table 1 and described in depth below.

### 1.2.1 Hydrated Mg-sulfates

All polyhydrated Mg-sulfates ( $n\text{H}_2\text{O} > 1$ ) have strong absorptions at 1.95  $\mu\text{m}$  caused by the vibration of structural water attached to the sulfate anion (Gendrin et al., 2005) and a strong drop in reflectance at wavelengths  $>2.3 \mu\text{m}$  characteristic of sulfates due to the strength of a broad absorption  $\sim 2.4 \mu\text{m}$  (Clark et al., 1990; Gendrin et al., 2005; Cloutis et al., 2006; Mangold et al., 2008; Viviano-Beck et al., 2014). The width and depth of the hydration feature at 1.95  $\mu\text{m}$  increases as the sulfate gains structural water as the mineral must restructure to accommodate the additional  $\text{H}_2\text{O}$ . Under ambient terrestrial conditions, polyhydrated Mg-sulfate is commonly found as epsomite ( $\text{MgSO}_4 \cdot 7\text{H}_2\text{O}$ ), but the hydration state is sensitive to relative humidity and Mg-sulfate can lose structural water after just minutes of exposure to a dry environment (Sheppard et al., 2022). The *Curiosity* rover identified starkeyite ( $\text{MgSO}_4 \cdot 4\text{H}_2\text{O}$ ) and kieserite ( $\text{MgSO}_4 \cdot \text{H}_2\text{O}$ ) at Gale crater (Chipera et al., 2023; Tutolo et al., 2025). Starkeyite is the thermodynamically predicted phase in the Martian shallow subsurface given modern temperature and relative humidity conditions, and likely formed via dehydration of a higher hydrate, like epsomite (Chipera and Vaniman, 2007; Chipera et al., 2023). Kieserite is stable under modern martian surface conditions and may have formed from warm fluids (Chipera and Vaniman, 2007; Wang et al., 2009). Kieserite's spectrum is distinct from polyhydrated Mg-sulfates because its 1.9  $\mu\text{m}$  hydration feature is strong, broad, and angular, yielding a "boxy" or reverse check-mark

shape spanning 1.9–2.1  $\mu\text{m}$ ; it also has a weaker but sharp 2.4  $\mu\text{m}$  feature caused by  $(\text{SO}_4)_2^-$  stretching vibrations (Cloutis et al., 2006).

## 1.2.2 Carbonates

The fundamental absorptions caused by vibrations of  $\text{CO}_3^{2-}$  in carbonate minerals are in the mid-infrared at 7.067 ( $\nu_3$ ), 9.407 ( $\nu_1$ ), 11.4 ( $\nu_2$ ), and 14.7  $\mu\text{m}$  ( $\nu_4$ ); in the near-infrared range, two combination and overtone absorptions of these fundamental vibrations are visible at 2.30–2.35  $\mu\text{m}$  ( $3\nu_3$ ) and 2.50–2.55  $\mu\text{m}$  ( $\nu_1+2\nu_3$ ) (Clark et al., 1990; Bishop et al., 2021). These are the main absorptions that are used to identify martian surface carbonates, as they are in the wavelength range of both CRISM (0.4–4.0  $\mu\text{m}$ , 18 m/pixel) and OMEGA (0.38–5.1  $\mu\text{m}$ , 0.4–5 km/pixel). Three smaller fundamentals at 1.85–1.87  $\mu\text{m}$ , 1.97–2.0  $\mu\text{m}$ , and 2.12–2.16  $\mu\text{m}$  are visible in laboratory data (Clark et al., 1990) but are unlikely to be distinguishable from orbit due to their weaker strength and conflicting atmospheric  $\text{CO}_2$  absorptions. All of these absorptions change position and shape among different types of carbonates. In particular, Mg-carbonates have absorptions at 2.30 and 2.50  $\mu\text{m}$ ; Fe-carbonates at 2.32 and 2.52  $\mu\text{m}$ ; Ca-Mg-carbonate (dolomite) at 2.32 and 2.52  $\mu\text{m}$ ; and Ca-carbonates at 2.34 and 2.54  $\mu\text{m}$  (Hunt and Salisbury, 1970; Gaffey, 1976; Gaffey, 1986; Ehlmann et al., 2008; Wray et al., 2011; Bridges et al., 2019; Horgan et al., 2020; Bishop et al., 2021).

Although the carbonate overtone bands at 3.45 and 3.9  $\mu\text{m}$  exhibit greater band depth than those at 2.3 and 2.5  $\mu\text{m}$ , their use is limited due to the susceptibility of these longer wavelengths to artifacts. Both CRISM and OMEGA data beyond  $\sim 2.7$   $\mu\text{m}$  suffer from increased noise and calibration challenges, including thermal background effects, residual atmospheric contributions, and detector nonlinearity. Additionally, CRISM's signal-to-noise ratio is over four times lower beyond 2.7  $\mu\text{m}$  (Murchie et al., 2007; Ehlmann et al., 2008), reducing the reliability of detections in this range. While the 3.4–3.9  $\mu\text{m}$  absorptions were initially used for early carbonate identifications (Ehlmann et al., 2008), subsequent studies have prioritized the 2.3 and 2.5  $\mu\text{m}$  absorptions due to their higher SNR, reduced susceptibility to instrumental artifacts, and placement in a relatively cleaner atmospheric window (Dhondiyal et al., 2023).

Three issues that may lead to under-identification of carbonate in orbital spectra are overlapping absorptions, the ubiquity of martian dust, and instrumental detection limits. In theory, the distinct spectral features of carbonates should be identifiable when present in abundances  $<1$  vol.% in ideal laboratory conditions when not mixed with minerals that have overlapping or conflicting absorptions (Bandfield et al., 2003; Orofino et al., 2009). However, absorptions by other minerals at similar wavelengths can partially or completely obscure the features of carbonates. For example, the 2.35  $\mu\text{m}$  band of some clay minerals can overlap and obscure the carbonate feature at 2.3  $\mu\text{m}$  while leaving other carbonate absorptions untouched (Bishop et al., 2008; Orofino et al., 2009).

The global distribution of martian dust and its ability to coat surfaces means that even in regions where carbonate-bearing rocks are present, their spectral signatures may be muted or masked. Martian dust is rich in nanophase iron oxides which cause reddening of the spectrum and reduce contrast in spectral features (Poulet et al., 2007; Bishop et al., 2002). The dust also contains phyllosilicates, sulfates, and carbonates, with features that

can overlap and obscure relevant absorptions (Bandfield et al., 2003; Bishop et al., 2002; Berger et al., 2016).

Detection limits impose an additional challenge. Orofino et al. (2009) estimate that in many Martian basins, carbonates likely constitute only 0.1–3.0 vol.% of the sediment, keeping them below the  $\sim 4$  vol.% detection threshold for instruments such as CRISM and OMEGA. Even if carbonate-bearing sediments are exposed, their weak spectral signatures may be further reduced by atmospheric effects, instrument noise, and the influence of fine-grained dust coatings. This highlights the difficulty of detecting low-abundance carbonates from orbit, even when using high-resolution spectral imaging.

## 1.3 Detections of martian carbonates

### 1.3.1 Meteorites

Several types of carbonates have been identified in martian meteorites (Mittlefehldt, 1994; McSween, 1994; Borg et al., 1999; Bridges and Grady, 2000; Bridges et al., 2001; Gyollai et al., 2019; Kijatani et al., 2023). Carbonate veins in the nakhlites that are mostly siderite formed  $<670$  million years ago (Bridges and Grady, 2000; Swindle et al., 2000). Strongly zoned carbonates in ALH84001 include magnesite, siderite, and ankerite, with their zoning point to evolving fluids, possibly through mixing or evaporation (Bridges et al., 2019). These carbonates in meteorites are low abundance,  $\sim 1$  vol.% (Bridges et al., 2019).

### 1.3.2 Orbital and *in situ* observations beyond Gale crater

Despite possessing strong spectral features and a clear formation pathway, the orbital record of martian carbonates is notably sparse (Bibring et al., 2005; Bibring et al., 2006; Milliken et al., 2009). Thermal evolved gas analysis in northern soils at the site of the Phoenix Lander suggested 3–6 wt.% carbonate, mostly likely Mg- or Fe-carbonates (Boynton et al., 2009; Sutter et al., 2012). Mg-carbonates were detected in martian dust (2–5 wt.%) using Thermal Emission Spectrometer data in the mid-infrared (6–30  $\mu\text{m}$ ) (Bandfield et al., 2003).

The Spirit rover observed Mg-Fe-carbonates in the Comanche outcrop in Gusev crater at high abundance,  $\sim 26$  wt.% of the outcrop (Morris et al., 2010). The carbonates were hypothesized to have formed from hydrothermalism associated with local volcanic activity. These *in situ* observations were later complemented by orbital observations that detected carbonates mixed with olivine at the sub-pixels scale in the Comanche outcrop (Carter and Poulet, 2012). The mineralogy of the carbonates here is similar to those observed in ALH84001. Uncertain carbonate (siderite) detection at Oxia Planum based on the 2.5  $\mu\text{m}$  feature alone (Mandon and Parkes Bowen, 2021) will be investigated with the upcoming Rosalind Franklin rover (Kereszturi et al., 2016).

Identification of carbonates in near-infrared wavelengths covered by the CRISM and OMEGA instruments has been challenging. Carbonates have been identified from orbit in CRISM data in a few locations, most commonly in association with impact craters (Wray et al., 2011; Sun and Milliken, 2015; Bultel et al., 2015). It is unclear whether cratering processes formed the carbonates via

hydrothermal processes or just exposed them from greater depths (Ehlmann et al., 2008; Edwards and Ehlmann, 2015).

The only regional carbonate unit thus far identified on Mars (Niles et al., 2013; Bridges et al., 2019) spans the areas of Syrtis Major, Nili Fossae, and Terra Tyrrhena southwest of the Isidis basin (Ehlmann et al., 2008; Mustard et al., 2008; Mustard et al., 2010; Edwards and Ehlmann, 2015). Its thickness appears to be 10 s of meters (Bramble et al., 2017) and its carbonate mineralogy is variable. Nili Fossae and west of Isidis Basin contains magnesite (Ehlmann et al., 2008), whereas uplifted Noachian crust in craters in Tyrrhena Terra appear to contain siderite. Weak detections of dolomite have been identified in Libya Montes (Ehlmann et al., 2008; Bishop et al., 2013). Ca- or Fe-carbonates have been exhumed by a crater near Syrtis Major (Michalski and Niles, 2010). Nearby Jezero crater has Mg-carbonates in basin-filling sediments and fluvio-deltaic deposits visible from orbit (Goudge et al., 2017; Stack et al., 2020) and Mg- and Ca-carbonates found *in situ* by the Perseverance rover (Horgan et al., 2020; Phua et al., 2024).

### 1.3.3 Carbonates in Gale crater

Despite recent improvements in spectral analysis algorithms and atmospheric detection, carbonates have not been orbitally identified in Gale crater (Sheppard et al., 2020; Sheppard et al., 2021; Dhoundiyal et al., 2023). However, *in situ* detections of carbonates of ~5–10 wt.% from the CheMin instrument (Tutolo et al., 2025) have repeatedly raised the question of why these spectrally distinct and environmentally important minerals are not seen from orbit in Gale. The Curiosity rover detected trace carbonate in Gale Crater (i.e., below orbital detections) in lower strata (Leshin et al., 2013; Archer, 2014; Ming et al., 2014; Yen et al., 2017). The Sample Analysis at Mars (SAM) instrument suite detected Fe-rich carbonates in aeolian deposits via evolved gas analysis (Sutter et al., 2017). CheMin had theorized about the presence of Fe-carbonates since this SAM detection, but it remained below CheMin detection limits until the clay-rich Glen Torridon unit, where Fe(II)-carbonate was detected in abundances of 1–3 wt.% in samples derived a few cm below the surface (Rampe et al., 2020; Thorpe et al., 2022).

More recently, CheMin observed siderite in the Mg-sulfate rich strata in the drill targets Tapo Caparo, Ubajara, and Sequoia in abundances as high as 10.5 wt.% (Table 2; Figure 1). These siderite detections are consistent with observations of a 400°C CO<sub>2</sub> release peak in SAM EGA data (Clark et al., 2024). Amorphous abundances are based on mass balance calculations performed using the chemical composition of the bulk sample, the chemical compositions of individual phases, and the relative proportions of those phases in the crystalline component (Blake et al., 2012; Blake and Morris, 2013). Fits of CheMin data model the entire diffraction pattern rather than individual peaks using FULLPAT<sup>1</sup>, including the scatter (i.e., enhanced noise above the background) from poorly ordered or amorphous materials (Thorpe et al., 2022; Chipera et al., 2023).

### 1.3.4 Sulfates in Gale crater

Sulfate minerals in Gale crater exhibit diverse mineralogical compositions, hydration states, and crystallinity, reflecting complex

aqueous histories. Monohydrated ( $\cdot 1\text{H}_2\text{O}$ ) and polyhydrated ( $\cdot 2 + \text{H}_2\text{O}$ ) sulfates have been identified through *in situ* and orbital data, with variations in hydration states indicating past fluctuations in water activity. These sulfates commonly occur as diagenetic features, including veins, nodules, and cemented horizons, suggesting post-depositional fluid interactions that altered primary sedimentary compositions (Nachon et al., 2017; Sun et al., 2019; Kronyak et al., 2019; Achilles et al., 2020). Spectrally, sulfates exhibit characteristic absorptions around 1.4  $\mu\text{m}$  and 1.9–2.1  $\mu\text{m}$  (indicative of structural water) and 2.4  $\mu\text{m}$  (S–O stretching in sulfate anions). The crystallinity of these phases varies, with some sulfates preserving well-defined crystalline structures, while others become X-ray amorphous, likely due to diagenetic recrystallization or alteration in low-water activity environments including exposure to modern surface conditions (Sheppard et al., 2022). The spatial distribution and stratigraphic occurrence of sulfates in Gale crater highlight their role as records of past aqueous alteration, episodic wetting events, and changing geochemical conditions during the crater's sedimentary evolution.

While many sulfates on the martian surface are thought to be primary deposits that formed as the planet dried out, recording large-scale desiccation events in the Hesperian period (Bibring et al., 2006), the complex diagenetic history of sulfates observed in Gale crater suggests that later processes can also generate or modify these minerals. Observations in Gale crater of Amazonian-aged jarosite, a ferric sulfate phase that typically forms in acidic, oxidizing conditions, indicates continued aqueous alteration well after initial sulfate deposition, likely driven by localized or transient fluid activity (Martin et al., 2017). These findings suggest that sulfate formation on Mars is not limited to a singular period of surface desiccation but may have continued episodically through diagenetic processes influenced by groundwater migration, ice interactions, and surface-atmosphere exchange. Recent work suggests that sulfate formation on Mars may still be occurring under present-day conditions through heterogeneous reactions involving microscopic interfacial water films, which can form in volcanic plumes or at ice-grain boundaries, allowing for aqueous oxidation of sulfur species even at subzero temperatures (Góbi and Kereszturi, 2019).

## 1.4 Laboratory experiments designed to investigate the lack of orbital carbonate signatures on Mars

Because of the proximity of Mg-sulfate- and carbonate-bearing materials in samples analyzed along the Curiosity traverse (as described above), we seek to identify whether the SO<sub>4</sub> and H<sub>2</sub>O related features in Mg-sulfates may spectrally mask the presence of Fe-carbonate in VNIR wavelengths when the two minerals are intimately mixed. While radiative-transfer modeling of spectral mixtures can reproduce checkerboard and intimate mixing spectra within 2% under certain conditions and mineral species, the ability to model abundances <10 wt.% is often challenging (Stack and Milliken, 2015; Robertson et al., 2016). We use exposure to a N<sub>2</sub>-purged environmental chamber under variable temperature to dehydrate the Mg-sulfates within the mixture, while collecting spectral images through time, to track how

1 doi: 10.1107/S0021889802017405

TABLE 2 CheMin-derived Mg-sulfate and carbonate abundances (in wt.%) for all drill targets that contain Mg-sulfate and carbonate above the CheMin detection limits. Errors are 1-sigma. Abundances are available in the planetary data system.

Drill target	Siderite	Ankerite	Starkeyite	Kieserite	Amorphous Mg-sulfate
GE <sup>a</sup>	0.8 ± 0.2				
KM <sup>a</sup>	2.2 ± 0.3				
MA <sup>a</sup>	1.4 ± 0.4				
MA3 <sup>a</sup>	1.1 ± 0.7				
GR <sup>a</sup>	3.2 ± 1.1				
NT <sup>b</sup>		0.9 ± 0.3			
BD <sup>b</sup>		1.0 ± 0.7			
CA <sup>c</sup>			2.3 ± 0.3		19 ± 4
TC <sup>d,e</sup>	10.5 ± 0.5			3.2 ± 0.4	16 ± 4
UB <sup>d,e</sup>	4.8 ± 0.3		6.4 ± 0.8		22 ± 5
SQ <sup>d,e</sup>	7.6 ± 0.4			5.8 ± 0.8	11 ± 3

Abundances from:

<sup>a</sup>Thorpe et al., 2022.

<sup>b</sup>Morrison et al., 2024.

<sup>c</sup>Chipera et al., 2023.

<sup>d</sup>Clark et al., 2024.

<sup>e</sup>Tutolo et al., 2025.

the presence of different Mg-sulfate hydration states affects the visibility of carbonate absorptions. Compared to spectral modeling, laboratory experiments are beneficial as they allow for the study of mixture spectra without needing to provide optical constant or textural information *a priori*. Similar experiments collecting spectra of mixtures throughout sample dehydration have shown that clay minerals can obscure spectral evidence of phyllosilicates using a point spectrometer (Sheppard et al., 2022). The detail of spectral images collected by MicrOmega allow us to ensure we are capturing areas within the mixture that contain both types of mineral grains, and to examine the spatial variability in spectra within the mixtures.

## 2 Methods

### 2.1 Sample selection and preparation

We created five physical mixtures of polyhydrated Mg-sulfate and siderite powders at different ratios by mass to examine whether Mg-sulfate can obscure the ~2.3 and 2.5 μm spectral absorption features most commonly used to map siderite from orbit in CRISM and OMEGA data (Table 3). We created mixtures with polyhydrated sulfate (epsomite at laboratory conditions) and not monohydrated Mg-sulfate because the sulfate unit in Gale crater has an orbital signature of polyhydrated Mg-sulfate.

The polyhydrated Mg-sulfate was purchased commercially and its composition and hydration state verified with FTIR spectroscopy (Figure 2). The siderite was a hand sample collected from Guizhou

Province, China that was powdered with an agate mortar and pestle and its composition was verified with FTIR spectroscopy (Figure 2). The grain size of both the Mg-sulfate and siderite spanned 250–700 μm (fine to coarse sand), which includes is an appropriate comparison for martian rocks (Rivera-Hernández et al., 2020). The samples were not sieved.

Samples were weighed with a balance and then physically mixed in glass sample vials to combine at the grain scale before placing in metal sample cups (total volume ~0.5 cm<sup>3</sup>, 3 mm thick) for analysis. When adding to the sample cup, care was taken to achieve a mix of both grains at the optical surface. Samples were gently leveled with a sheet of weighing paper to ensure a relatively smooth sampling surface for imaging.

### 2.2 FTIR spectrometer

Both starting materials were analyzed on a Fourier Transform IR (FTIR) spectrometer (Perkin Elmer Spectrum 100 N) under ambient temperature and pressure conditions with a spectral resolution of 4 cm<sup>-1</sup>. For reflectance spectroscopy, the system uses biconical reflectance (the incoming light is projected to an ellipsoid mirror and focused onto the sample, then scattered and the diffuse part is collected by another ellipsoid mirror—the Selector Diffuse Reflectance Accessory by Specac).

This spectrometer was used to confirm their composition before beginning the experiment with MicrOmega. FTIR spectra were collected against diffuse gold standard and Spectralon white reference from Labsphere.

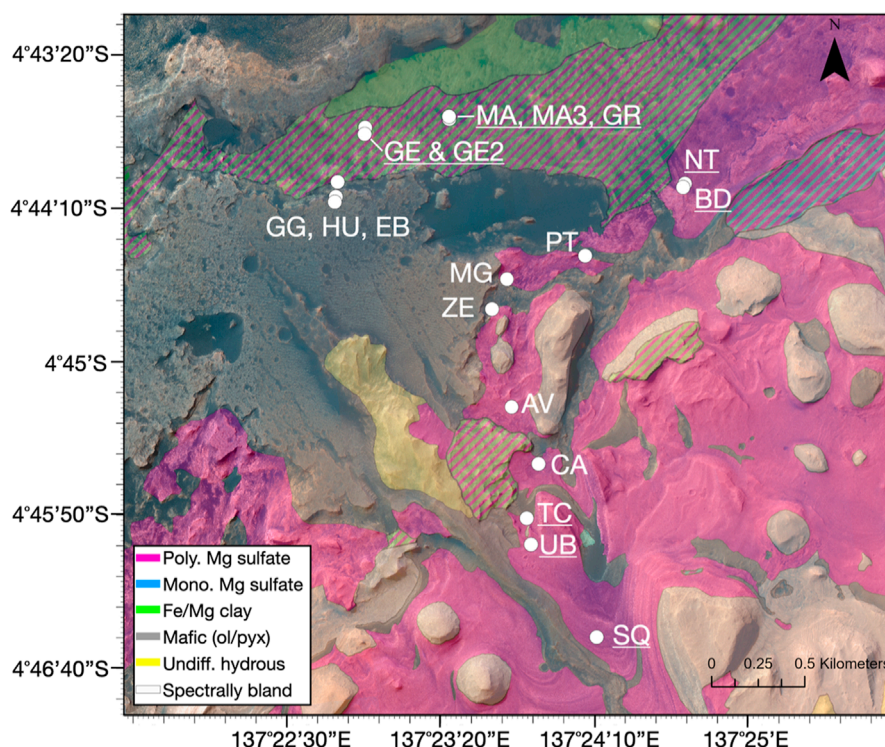


**FIGURE 1** Orbital map of relevant Curiosity rover drill holes. Samples where Curiosity detected Fe(II)-carbonate with CheMin are underlined: Glen Etive (GE, sol 2486), Mary Anning (MA, sol 2838), Mary Anning 3 (MA3, sol 2870), Groken (GR, sol 2912) (Thorpe et al., 2022), Nontron (NT, sol 3056), Bardou (BD, sol 3094), Tapo Caparo (TC, sol 3752), Ubajara (UB, sol 3823), and Sequoia (SQ, sol 3980). Targets where Fe(II)-carbonate was not detected are not underlined: Glasgow (GG), Hutton (HU), Edinburgh (EB), Pontours (PT), Maria Gordon (MG), Zechstein (ZE), Avanavero (AV), and Canaima (CA). The drill holes are superimposed over HiRISE images and an updated version of the mineral map based on CRISM data presented by Sheppard et al. (2020), with polyhydrated Mg-sulfate mapped in pink.

**TABLE 3** Contents of the 5 physical mixtures analyzed in this work. Each physical mixture was analyzed at 3 timepoints ( $t_0$ ,  $t_1$ ,  $t_2$ ).

% Mg-sulfate	% siderite	Sample number at $t_0$	Sample number at $t_1$	Sample number at $t_2$
100	0	1	6	11
75	25	2	7	12
50	50	3	8	13
25	75	4	9	14
0	100	5	10	15

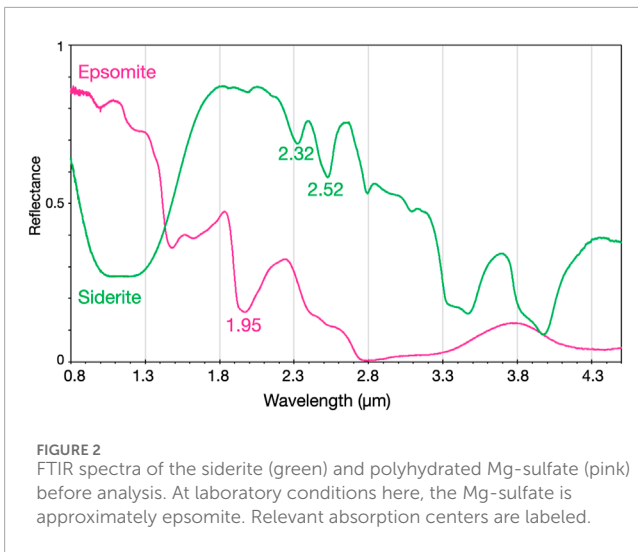
## 2.3 MicrOmega imaging spectrometer

### 2.3.1 Instrument setup

MicrOmega is an infrared (0.99–3.65  $\mu\text{m}$ ) hyperspectral microscope with a FoV of  $5 \times 5$  mm, a pixel size of  $\sim 22$   $\mu\text{m}$ , and a spectral resolution of  $20 \text{ cm}^{-1}$  (Bibring et al., 2017), originally developed for the ExoMars Rosalind Franklin rover. The instrument used in this study is a flight-spares (FS) model of MicrOmega.

For the safety of the instrument, and to optimize the observational conditions of multiple samples, a dedicated and semi-automated setup “PTAL chamber” (Planetary Terrestrial

Analogue Library) was built for the use of the MicrOmega instrument (Loizeau et al., 2020). The PTAL chamber consists of a large glove box flushed with pure  $\text{N}_2$ , within which MicrOmega is installed in a dedicated box also flushed with  $\text{N}_2$  at higher pressure. A movable platform allows the precise position of the sample under MicrOmega FS. MicrOmega FS interface and the sample stage can be cooled down to about  $-20^\circ\text{C}$  each to allow better signal/noise and to mimic Martian conditions. Samples are put into the glovebox through an air-lock that can be also flushed with  $\text{N}_2$ . Operating under  $\text{N}_2$  purged atmosphere avoids any dust settling and any water condensation or ice on the instrument and samples. In addition,



within the airlock, a small setup can be used to heat the samples to 100°C to help drying them.

This setup allows for repeated spectral image collection (capturing spatial variability) during dehydration of samples (capturing temporal variability).

### 2.3.2 Sample measurement

The five samples were added to 1 cm diameter gold-plated copper sample cups, and MicrOmega spectra were collected against a diffuse gold standard (Infragold<sup>®</sup>) and a homogeneous bright standard (Spectralon<sup>®</sup> 99%) for radiometric calibration. We collected MicrOmega spectral image cubes of each sample at three exposure times: 0 h ( $t_0$ ), 3 h ( $t_1$ ), and 1 month ( $t_2$ ) to capture changes in spectral signatures induced by the dehydration of polyhydrated Mg sulfate at dry conditions. Samples remained in the MicrOmega N<sub>2</sub>-purged instrument chamber (RH<0.1%) during the entirety of the experiment.

During the measurement of spectra at  $t_0$ , the sample stage was set to -23°C to slow dehydration of the polyhydrated Mg-sulfate samples, which were measured first given its capability for rapid dehydration and subsequent mineralogical restructuring; the siderite sample was measured last. After  $t_0$  and before measurement of spectra at  $t_1$ , samples were brought to the N<sub>2</sub> purged airlock and heated to 100°C to encourage the loss of structural water from the Mg-sulfate. Both sample heating and exposure to N<sub>2</sub> dry air have been shown to remove structural water from polyhydrated Mg-sulfate within minutes (Sheppard et al., 2022). The samples were then stored in the N<sub>2</sub> purged glovebox for 1 month before collection of the spectra at  $t_2$  at ambient temperature after 1 month of continuous exposure to dry air.

### 2.3.3 Post-processing and analysis

After MicrOmega data calibration similar to the one used by Riu et al. (2022), we calculated relevant spectral parameters to aid in identification of specific grains within the mixture and investigated the spectra individually to look for features visible at the grain ( $\mu\text{m-mm}$ ) and image ( $5 \times 5 \text{ mm}$ ) scales. Here we focus on the spectral parameters SINDEXT2 which measures the drop in reflectance and

resulting convexity of spectral shape seen in sulfates >2.1  $\mu\text{m}$ , and MIN2345\_2537 which measures the two carbonate absorptions at 2.345 and 2.537  $\mu\text{m}$  frequently seen in Fe-carbonates (Viviano-Beck et al., 2014). Spectral parameter maps were stretched to 0–0.5 such that only positive detections in an image were highlighted, which was used to identify distinct mineral grains and clumps of grains for analysis. Spectral parameters were calculated using the CAT 7.4 package for ENVI, available from the PDS Geosciences Node. Calculation of SINDEXT2 (Equation 1) takes the median over 5 channels around R2120; 7 channels around R2290; and 3 channels around R2400; calculation of MIN2345\_2537 (Equation 2) takes the median over 5 channels surrounding all reflectance values (Viviano-Beck et al., 2014).

$$\text{SINDEXT2} = 1 - \left( \frac{a * R2120 + b * R2400}{R2290} \right) \quad (1)$$

$$\text{MIN2345\_2537} = \text{minimum} \left[ \left( 1 - \left( \frac{R2345}{a * R2250 + b * R2430} \right) \right), \left( 1 - \left( \frac{R2537}{a * R2430 + b * R2602} \right) \right) \right] \quad (2)$$

## 3 Results

### 3.1 FTIR spectra

The Mg-sulfate at laboratory conditions as measured on the FTIR spectrometer has features consistent with epsomite. This includes the defined doublet appearance of the 1.4  $\mu\text{m}$  (H<sub>2</sub>O), as well as a strong 1.93–1.95  $\mu\text{m}$  (H<sub>2</sub>O), weak 0.97 and 1.15  $\mu\text{m}$  absorptions (H<sub>2</sub>O overtones), and a strong drop in reflectance after ~2.3  $\mu\text{m}$  (Figure 2; Wang et al., 2011; Chou et al., 2013; Clark et al., 1990; Gendrin et al., 2005; Cloutis et al., 2006). Epsomite at ambient conditions has been observed in other laboratory experiments (Sheppard et al., 2022).

The siderite has absorption features consistent with pure-Fe(II) carbonates described above: strong combination and overtone absorptions at 2.32, 2.52, 3.4, and 3.9  $\mu\text{m}$  (Figure 2). Siderite is nominally anhydrous, but the natural sample we used has small vibrational OH absorptions at 2.79 and 3.09  $\mu\text{m}$  that are likely due to surface weathering not fully removed during sample preparation. The weathering products are likely hydrated Fe-carbonate or Fe-bearing (oxy)hydroxides.

### 3.2 MicrOmega spectral parameter maps

Exposure to the MicrOmega dry chamber resulted in physical and spectral changes to the sulfate-bearing samples.

Spectral parameter maps of the image cubes of the five physical mixtures can be used to distinguish Mg-sulfate and siderite grains by identifying spatially coherent areas with consistently high values of the two relevant spectral parameters SINDEXT2 and MIN2345\_2537, respectively (Figure 3). SINDEXT2 measures the spectrum convexity seen in sulfates rather than the hydration bands, which is why the SINDEXT2 values do not change much in Figure 3 despite the individual spectra changing as the sulfate dehydrates (Figure 4). Mg-sulfate in the samples at  $t_0$  and  $t_1$  have higher values of the SINDEXT2 parameter. At  $t_2$ , Mg-sulfate appears somewhat texturally condensed

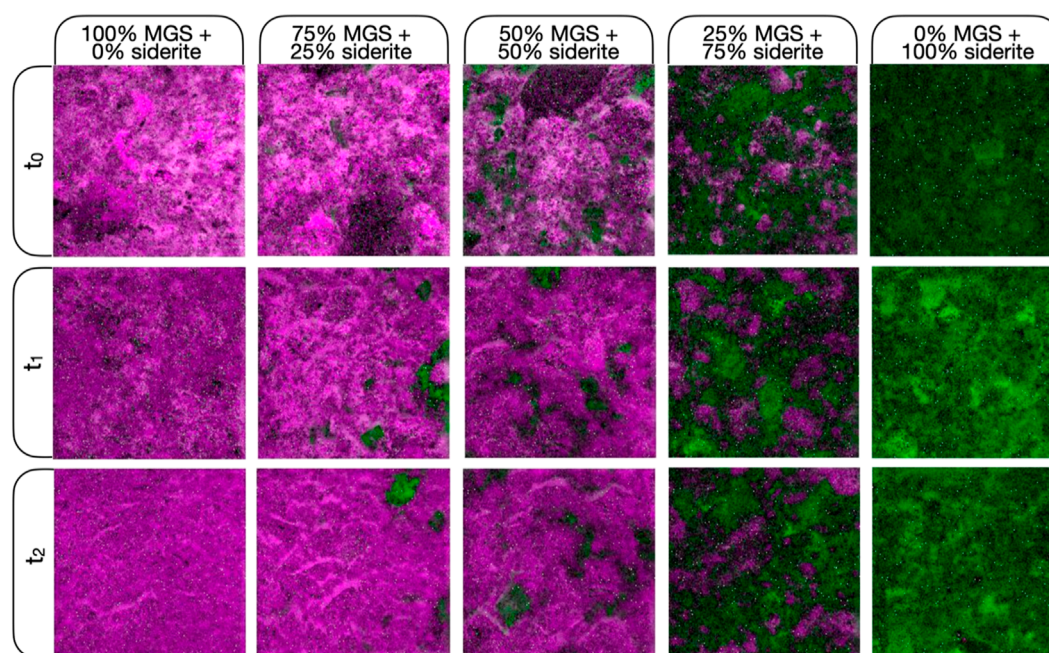


FIGURE 3

Complete MicrOmega infrared images ( $5 \times 5$  mm) of all physical mixtures (columns) at three times (rows) where  $t_0$  is immediate at initial laboratory conditions,  $t_1$  is 3 h, and  $t_2$  is 1 month. The physical sample remains the same between time steps but the FOV of the image changes as  $5 \times 5$  mm is only a portion of the sample cup size. SINDEXT2 is mapped here in the red and blue channels such that large SINDEXT2 values (convexity at  $2.29 \mu\text{m}$  due to  $2.1$  and  $2.4 \mu\text{m}$  absorptions which are attributed to Mg-sulfate grains) are shown in magenta. MIN2345\_2537 spectral parameter shown in green, highlighting siderite grains in the mixture. Spectral parameters are stretched identically in all images (0–0.5).

into a tiger-stripe texture as it loses volume due to exposure to the dry chamber. The 100% siderite samples appear identical as siderite is nominally anhydrous and should not dehydrate in the chamber through time. While there does appear to be a minor weathering component noted above in the FTIR spectrum causing OH absorptions at  $2.79$  and  $3.09 \mu\text{m}$ , this should have little effect on these observations that are based on the SINDEXT2 and MIN2345\_2537 parameters. Siderite grains in some mixtures are seen as bright green in these parameter maps (high MIN2345\_2537 values), while in some samples they appear relatively black (low MIN2345\_2537 values) and are only identifiable as voids in the SINDEXT2 signal, implying that their spectra are less consistent with carbonate features.

### 3.3 MicrOmega spectra

#### 3.3.1 Mg-sulfate dehydrates in the MicrOmega chamber

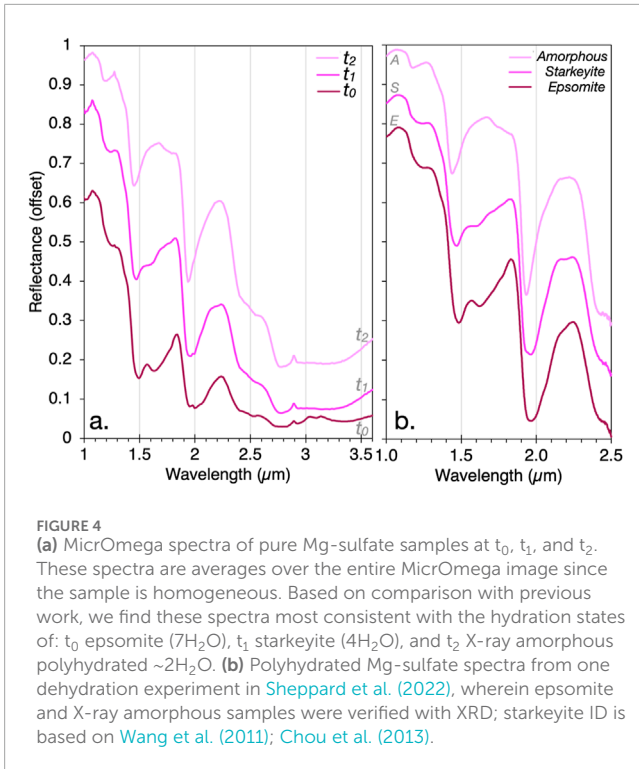
The dehydration of Mg-sulfate due to exposure to the MicrOmega chamber is also reflected in the individual pixel spectra (Figure 4). The approximate hydration state of Mg-sulfate can be identified using the shape and position of the hydration bands in Mg-sulfate (Wang et al., 2011; Chou et al., 2013; Sheppard et al., 2022). The  $t_0$  Mg-sulfate is consistent with epsomite ( $7\text{H}_2\text{O}$ );  $t_1$  is most consistent with starkeyite ( $4\text{H}_2\text{O}$ ); and  $t_2$  is most consistent with hydrated X-ray amorphous Mg-sulfate

( $\sim 2\text{H}_2\text{O}$ ). This is consistent with previous work (Wang et al., 2011; Chou et al., 2013; Sheppard et al., 2022).

#### 3.3.2 The $2.3$ and $2.5 \mu\text{m}$ carbonate absorptions

The two dominant features currently used for orbital identification of carbonates in CRISM and OMEGA datasets, the  $2.3$  and  $2.5 \mu\text{m}$  absorptions, are affected differently in our experiments. We find that the  $2.5 \mu\text{m}$  absorption is consistently observable in all the samples containing siderite, but the  $2.3 \mu\text{m}$  feature can only be resolved in localized analyses ( $5 \times 5$  pixel average) focusing on individual siderite grains (Figure 5). However, when the image is averaged ( $150 \times 150$  pixel average), which is more analogous to orbital observations where pixels likely contain mixed mineralogy, the  $2.3 \mu\text{m}$  feature is no longer identifiable (Figure 5, black spectra). This suggests that the  $2.3 \mu\text{m}$  absorption is more susceptible to dilution by other phases in a mixed spectral signal, whereas the  $2.5 \mu\text{m}$  feature remains more resilient to spectral mixing effects. One possible explanation is that the  $2.3 \mu\text{m}$  band is intrinsically weaker and may be masked by the strong slope in this spectral region, from the local maximum at  $2.2 \mu\text{m}$  to the strongly absorbing  $3 \mu\text{m}$  region.

This can also be seen in measures of SINDEXT within sulfate, MIN2345\_2537 within sulfate, and the band depth at  $2.52$  (BD at  $2.52$ ) within carbonate (Table 4). These constitute high values within each image. BD at  $2.52$  was calculated using Equation 3 (Clark and Roush, 1984) with a continuum spanning  $2.40$ – $2.61 \mu\text{m}$ . For calculation of the two spectral parameters of carbonate grains, MIN2345\_2537 and BD at  $2.52$ , the images were linked so that the



same grain was used, allowing for direct comparison.

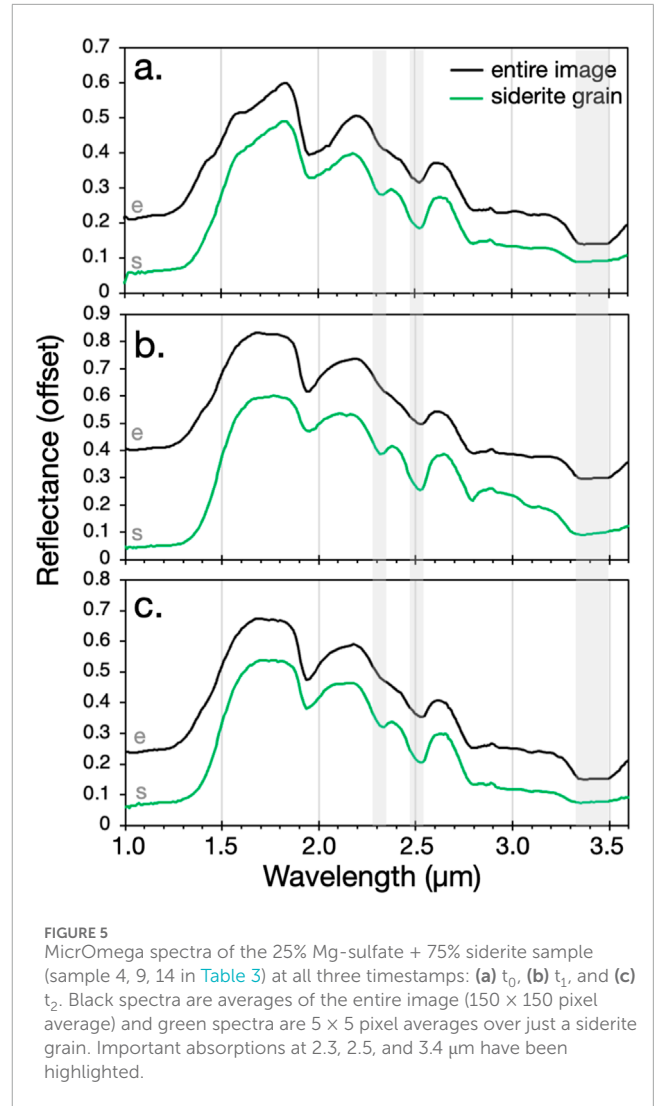
$$\text{BandDepth} = 1 - \left( \frac{b_2}{\frac{b_1 + b_3}{2}} \right) \quad (3)$$

Within Table 4, it can be seen that SINDEXT2 is higher in the samples which have a higher proportion of sulfate. For one sample measured through time, SINDEXT2 is also slightly higher in  $t_0$  than in  $t_1$ , and slightly higher in  $t_1$  than in  $t_2$ , as the dehydration of sulfate decreases the contrast between reflectance before and after  $2.2 \mu\text{m}$ , part of what SINDEXT2 is calculating. For the carbonate spectral parameters, it can be seen that both spectral parameters are highest for the 100% carbonate samples. Further implications of these two carbonate spectral parameters are discussed in Section 4.3.

We also note that the  $2.79 \mu\text{m}$  feature seen in the FTIR spectrum from the ambient sample (Figure 2) is visible in the individual siderite grain at  $t_1$  spectrum (Figure 5b). Because of the movable sample stage, MicrOmega images are collected over different areas of the sample cup at each timepoint, meaning this grain may have a small weathering component. We believe this does not affect the rest of the spectrum or results.

### 3.3.3 Conditions under which siderite spectra are obscured

We find that if the Mg-sulfate in the mixture is crystalline epsomite ( $t_0$ ), spectral evidence of siderite is easily lost, with the  $2.3$ ,  $3.4$ , and  $3.9 \mu\text{m}$  absorptions essentially absent and only a small  $2.5 \mu\text{m}$  absorption visible (Figure 6a). We find that the presence of less hydrated starkeyite ( $t_1$ , Figure 6b) and amorphous ( $t_2$ , Figure 6c) forms of Mg-sulfate are less capable of obscuring the spectral features of siderite grains at the  $5 \times 5$  pixel level, likely due to the



effects of scattering within the mixture, and that absorptions at the  $2.3$ ,  $2.5$ ,  $3.4$ , and  $3.9 \mu\text{m}$  are visible in some of these spectra.

This loss of distinctive siderite absorptions ( $2.3$ ,  $2.5$ ,  $3.4$ , and  $3.9 \mu\text{m}$ ) is also seen in whole-image average spectra of all three physical mixtures of Mg-sulfate and siderite (Figure 7).

## 4 Discussion

### 4.1 MicrOmega spectra highlight the spatial variability in sulfate-carbonate mixture spectra

Even in high carbonate abundance mixtures (75 wt%), we find that the  $2.3 \mu\text{m}$  absorption is lost in the presence of sulfate unless analysis focuses on pixels from just a carbonate grain without the influence of sulfate grains (Figure 5), which is unlikely in Mars orbital spectra.

In low carbonate abundance mixtures (25 wt%), crystalline polyhydrated Mg-sulfate is able to obscure the spectral evidence of carbonate even when carbonate grains are focused on alone

TABLE 4 Example elevated spectral parameter values from within grains in each experiment.

Experiment number	Mineral mixture (sulfate:carbonate)	Time	SINDEX of sulfate	MIN2345_2537 of carbonate	BD at 2.52 of carbonate
1	100:0	$t_0$	0.553366	—	—
2	75:25	$t_0$	0.546538	0.074922	0.261240
3	50:50	$t_0$	0.455088	0.074631	0.367656
4	25:75	$t_0$	0.337388	0.103640	0.362645
5	0:100	$t_0$	—	0.151379	0.484378
6	100:0	$t_1$	0.415020	—	—
7	75:25	$t_1$	0.462825	0.102548	0.429831
8	50:50	$t_1$	0.378435	0.103346	0.430588
9	25:75	$t_1$	0.256625	0.108582	0.389427
10	0:100	$t_1$	—	0.196760	0.492926
11	100:0	$t_2$	0.369405	—	—
12	75:25	$t_2$	0.386530	0.154200	0.430,546
13	50:50	$t_2$	0.334192	0.088912	0.305540
14	25:75	$t_2$	0.299312	0.104369	0.363476
15	0:100	$t_2$	—	0.157005	0.508029

for analysis (Figure 6a). If sulfate and carbonate grains both contribute to the spectra, at least three distinct hydration states and crystallinities of Mg-sulfate are capable of obscuring carbonate spectra (Figure 7a). This effect may be due to multiple scattering within the intimately mixed grains, which enhances the spectral dominance of the sulfate. This is consistent with past work showing that intimate mixtures of hydrated sulfates can obscure the spectral evidence of other components, such as chloride salts (Ye and Glotch, 2019; Hughes et al., 2023), nitrates, or carbonates (Sutter et al., 2007).

While the dehydration of Mg-sulfate will result in changes to wt% and vol% within the sulfate-carbonate physical mixtures, this does not appear to be driving these changes in spectra through time. The 2.5  $\mu\text{m}$  absorption at  $t_0$  is slightly stronger than at  $t_1$  or  $t_2$  (Figures 7b, c), while the opposite would be expected if the smaller volumetric proportion of the Mg-sulfate were driving the changes in spectral signatures.

## 4.2 Mg-sulfate may be the reason gale crater carbonates are not visible from orbit

All the drill holes where siderite has been identified in Gale crater are in areas orbitally mapped as polyhydrated Mg-sulfate (Figure 1). Given the laboratory results in Figures 6, 7, it is conceivable that crystalline or amorphous polyhydrated Mg-sulfate

is obscuring the absorption features used to map siderite in CRISM and OMEGA data.

Three drill targets that span nearly 90 m of elevation change within the sulfate unit in Gale crater have crystalline and X-ray amorphous Mg-sulfate and Fe(II)-carbonate. Going up section, TC has kieserite, amorphous Mg sulfate, and siderite; UB has kieserite, amorphous Mg sulfate, and siderite; and SQ has kieserite, amorphous Mg sulfate, and siderite (Chipera et al., 2023; Tutolo et al., 2025; Table 2). Chipera et al. (2023) calculated the hydration state of amorphous Mg-sulfate in the Canaima drill target, drilled from the base of the sulfate unit and devoid of carbonate in CheMin data. These calculations suggest the amorphous Mg-sulfate measured by CheMin contains 3.2  $\text{H}_2\text{O}$  per formula unit. Based on our laboratory measurements, we hypothesize that both crystalline and amorphous polyhydrated Mg-sulfate can obscure siderite absorption bands in CRISM data.

An important difference between CheMin and CRISM mineral detections is the depth of the materials being interrogated. CheMin measures drill powder from a depth of  $\sim 4$  cm, whereas CRISM measures the top few micrometers of the martian surface, which can be affected by dust cover and diurnal temperature and relative humidity variations. Starkeyite is likely the most prevalent crystalline polyhydrated Mg-sulfate just below the martian surface at depths sampled by Curiosity. However, at the uppermost surface, exposure to solar heating and varying temperature and humidity may cause some starkeyite to partially dehydrate and transition to

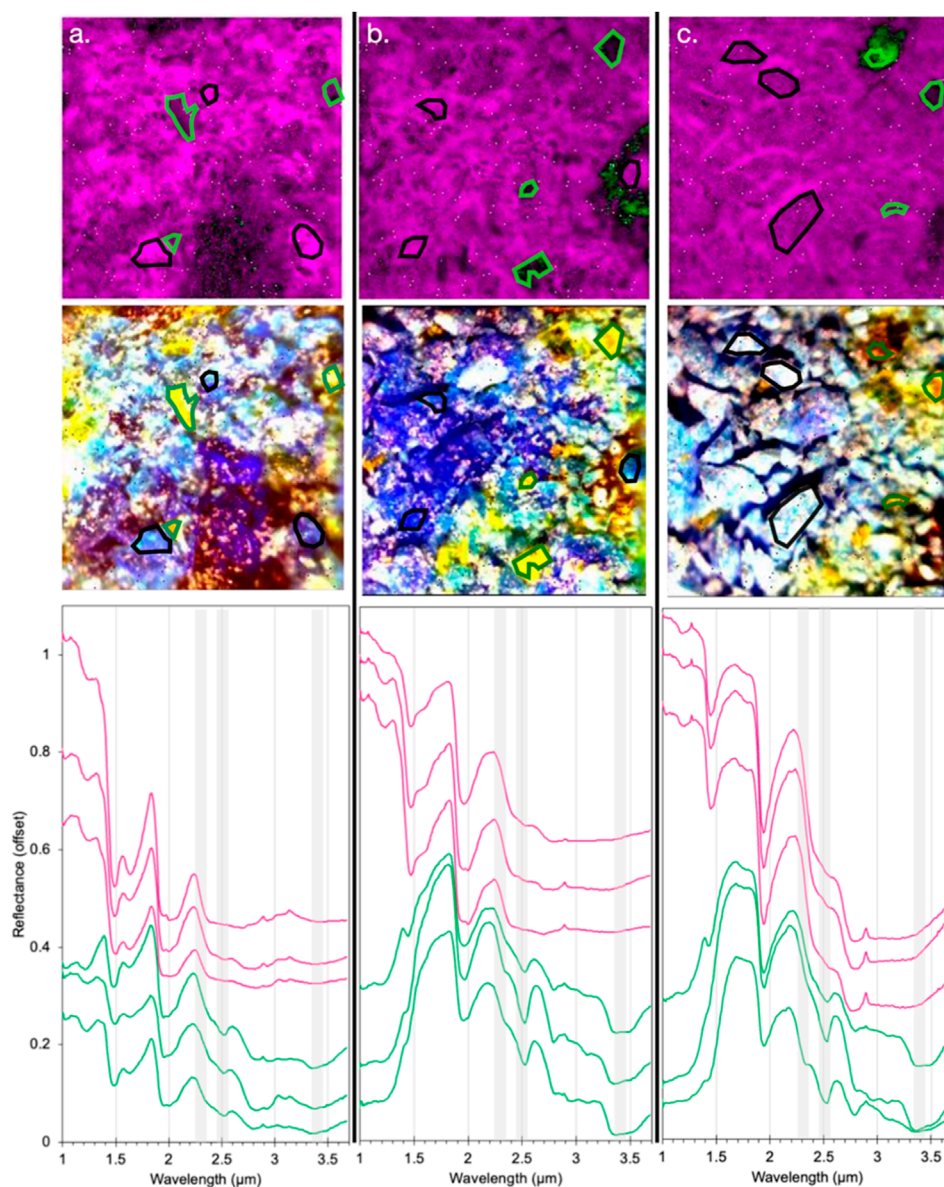


**FIGURE 6**

MicrOmega images and region of interest (ROI) spectra of three physical mixtures: **(a)** Sample 2: 75% MGS + 25% siderite at  $t_0$ , **(b)** Sample 7: 75% MGS + 25% siderite at  $t_1$ , **(c)** Sample 12: 75% MGS + 25% siderite at  $t_2$ . The top row shows the SINDEX2 and MIN2345\_2537 image from Figure 3. The middle row shows a false-color image (Red: reflectance at 2.6  $\mu\text{m}$ , Green: reflectance at 2.2  $\mu\text{m}$ , and Blue: reflectance at 1.1  $\mu\text{m}$ ) that helps highlight individual siderite (appear yellow) and sulfate (appear blue) grains. The bottom row shows mean ROI spectra highlighted in each MicrOmega image. Pink spectra (top 3 spectra) are sulfate spectra from the ROIs highlighted in black. Green spectra (bottom 3 spectra) are siderite spectra from the ROIs highlighted in green. Important absorptions at 2.3, 2.5, and 3.4  $\mu\text{m}$  have been highlighted.

amorphous polyhydrated Mg-sulfate. Therefore, both starkeyite and amorphous Mg-sulfate are expected to be present at the martian surface, consistent with recent observations (Chipera et al., 2023).

Amorphous Mg-sulfate is also observed in CheMin measurements from the subsurface, but in this case it is likely a result of an additional phase transition induced during analysis inside the rover where elevated temperatures and reduced relative humidity can drive further dehydration of starkeyite to the amorphous phase. Thus, while amorphous Mg-sulfate is naturally present at the surface due to environmental exposure, some of it may also form artificially during sample processing within the rover.

It is possible that the absence of siderite features may be related to the abundance of hydrated Mg-sulfate in upper Mt. Sharp. Other features of Mt. Sharp may contribute to this lack of orbital carbonate features, such as the small volumetric proportion of carbonates, textural effects such as grain size or surface roughness, and dust cover. Mg-sulfate deposits elsewhere on the planet could similarly mask 2.3 and (to a lesser extent) 2.5  $\mu\text{m}$  absorptions related to carbonate if it is present at  $\sim 25$  wt.% (e.g., Figure 6) meaning the abundance of carbonate on the martian surface might be much higher than expected from orbital measurements. This is consistent with Tutolo et al., 2025, which proposed that the major

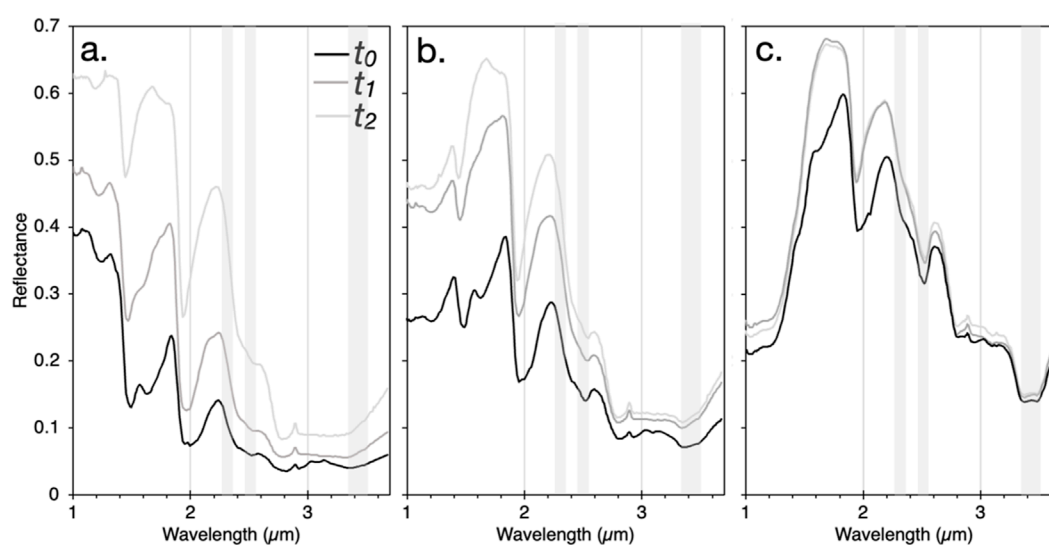


FIGURE 7

MicrOmega spectra of physical mixtures at  $t_0$ ,  $t_1$ , and  $t_2$ . All spectra are averages over the entire image ( $150 \times 150$  pixels) so include spectra influence of both Mg-sulfate (MGS) and siderite grains. (a) Samples 2, 7, 12: 75% MGS + 25% siderite. (b) Samples 3, 8, 13: 50% MGS + 50% siderite. (c) Sample 4, 9, 14: 25% MGS + 75% siderite. Important absorptions at 2.3, 2.5, and 3.4  $\mu\text{m}$  have been highlighted.

layered polyhydrated and monohydrated sulfate deposits may have carbonates at the abundances seen in Gale crater.

### 4.3 The orbital search for carbonates on Mars should revisit images, searching for the 2.5 $\mu\text{m}$ feature alone

We see that when the image is averaged ( $150 \times 150$  pixels averaged into one spectrum), which would be more analogous to orbital observations where pixels are likely to have mixed mineralogy, the 2.3  $\mu\text{m}$  feature are more difficult to identify, even in samples with 75% siderite (Figure 5, black spectra). The finding that the 2.5  $\mu\text{m}$  absorption is easier to resolve than the 2.3  $\mu\text{m}$  absorption in these mixtures suggests that in a CRISM pixel ( $18 \text{ m} \times 18 \text{ m}$ ) with Mg-sulfate present, it is likely the 2.3  $\mu\text{m}$  feature would be difficult to rely upon for a confident carbonate detection. In Table 4, we show that the siderite grains have consistently higher BD at 2.52  $\mu\text{m}$  values than MIN2345\_2537. This makes sense as MIN2345\_2537 is essentially the minimum of the two band depths at 2.345  $\mu\text{m}$  and 2.537  $\mu\text{m}$  (Equation 2). However, it also demonstrates our point that relying on MIN2345\_2537 and the presence of both absorptions to identify martian carbonates, especially in the presence of sulfates, may yield under-detection of carbonates. Indeed, Figure 8 updates the approach shown in Figure 3 by identifying carbonate grains using BD at 2.52  $\mu\text{m}$  instead of MIN2345\_2537. The carbonate spectral parameter values are overall higher (also seen in Table 4), and there are fewer “void” spaces where carbonate grains can only be identified by a lack of SINDEXT2 values.

Current spectral parameter maps and algorithmic methods of searching for martian surface carbonates rely on the search for both absorptions for a positive detection (Viviano-Beck et al., 2014; Dhoundiyal et al., 2023; Stepcenkov et al., 2022). In areas

with sulfates, the 2.5  $\mu\text{m}$  feature should be examined closely for the possibility of indicating the presence of carbonates. Given the uncertain carbonate detections at Oxia Planum and other locations that are based only on a 2.5  $\mu\text{m}$  absorption with no 2.3  $\mu\text{m}$ , it is important to revisit surface spectra to look for 2.5  $\mu\text{m}$  features alone, especially within scenes that also have polyhydrated sulfates (Mandon and Parkes Bowen, 2021). As one of the most common secondary minerals on Mars, this affects many orbital images that can be reexamined. When doing this, care should be taken to identify a distinct, sharp 2.5  $\mu\text{m}$  band so as to not misidentify other surface minerals with a 2.5  $\mu\text{m}$  absorption as potential carbonates (Bishop et al., 2021). This includes clay minerals (including certain smectites, serpentines, chlorites) and sulfates which can have broader absorptions and shoulders at 2.5  $\mu\text{m}$  related to structural OH combination stretching + bending vibrations (Ehlmann et al., 2008; Bishop et al., 2008).

The environmental implications for coexisting sulfates and carbonates remain an area of investigation on Mars. It may point to multiple generations of fluid or fluid evolution over time, as both generally require water to form and sulfates have been seen to be part of a complex history of multiple diagenetic events in Gale crater (Nachon et al., 2017; Sun et al., 2019; Kronyak et al., 2019; Achilles et al., 2020). The purity of siderite analyzed by CheMin in the sulfate unit and the absence of cation substitution for  $\text{Fe}^{2+}$  in the siderite structure demonstrates the fluids from which the siderite precipitated were enriched in  $\text{Fe}^{2+}$ . The lack of  $\text{Mg}^{2+}$  or  $\text{Ca}^{2+}$  in the siderite structure and the co-occurrence of Mg-sulfate and Ca-sulfate in the siderite-bearing rocks may indicate the sulfates formed from different fluid events (Tutolo et al., 2025). Alternatively, in the eolian-dominated depositional environments preserved in the sulfate unit, these minerals could have been mixed together physically. In the absence of petrographic information, it is difficult to definitively

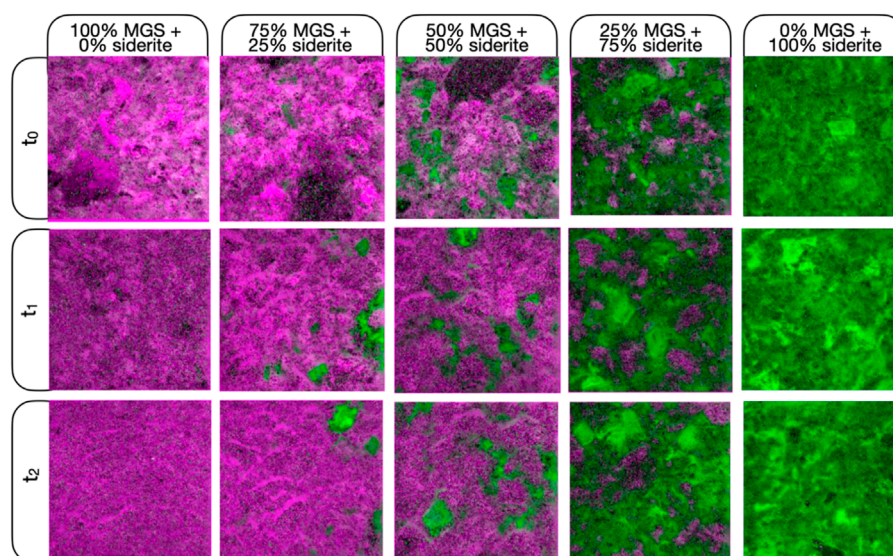


**FIGURE 8**  
A version of [Figure 3](#) except now the green channel is mapping BD at 2.52  $\mu\text{m}$  instead of MIN2345\_2537. Spectral parameters are stretched identically in all images in both [Figures 3, 8](#) (0–0.5).

determine the aqueous processes that led to the precipitation of carbonate and Mg-sulfate in the same rocks. Mars Sample Return and the delivery of samples from Mars to laboratories on Earth can help address the timing of secondary mineral precipitation and the conditions under which different phases formed. Carbonates and sulfates have been found in some drill cores collected by the Perseverance rover in Jezero crater (e.g., [Siljeström et al., 2024](#)), and analyses of the physical relationships between these phases, along with their crystal chemistries and isotopic compositions in terrestrial laboratories will flesh out the carbonate-sulfate history in at least one location on Mars.

Our finding that hydrated Mg-sulfate may obscure carbonate detections on Mars has important implications for the atmospheric density and C cycle on early Mars. Not only could Mg-sulfate be acting as an enormous sink for the martian water budget ([Vaniman et al., 2004](#); [Robertson and Bish, 2013](#)), it could also be obscuring the complete extent of a mineral class that is central to the planet's aqueous history. It is important to properly identify the extent of carbonates as it is used to constrain past atmospheric thickness and aqueous conditions in the Noachian.

## 5 Conclusion

Our laboratory experiments show that both crystalline and amorphous Mg-sulfate can obscure the 2.3  $\mu\text{m}$  siderite absorption band in the VNIR spectrum. We found that if sulfate and carbonate grains both contribute to the spectra, as is more analogous to Mars orbital spectra including CRISM and OMEGA, at least three distinct hydration states and crystallinities of Mg-sulfate are capable of obscuring carbonate spectral signatures even in high carbonate abundance mixtures (75 wt%). The 2.3  $\mu\text{m}$  carbonate absorption is especially easily obscured in the presence of sulfate unless analysis

focuses on an isolated carbonate grain. In low carbonate abundance mixtures (25 wt%), crystalline polyhydrated Mg-sulfate is able to obscure the spectral evidence of carbonate even when carbonate grain spectra are isolated.

These results have critical implications for Mars' surface mineralogy. The findings help explain why Fe(II)-carbonates detected *in situ* by the Curiosity rover in Gale Crater remain invisible in orbital data despite recent advances in orbital spectral processing. The co-occurrence of siderite with Mg-sulfate in several Gale Crater drill targets suggests that sulfates may be masking carbonates in orbital data. These results are also consistent with [Tutolo et al., 2025](#), which proposed that major layered sulfate deposits may have carbonates at the abundances seen in Gale crater. This spectral obscuration is particularly evident when analyzing large pixel averages that mimic the spatial resolution of orbital spectrometers.

The results emphasize the need to revisit orbital datasets with a focus on detecting the 2.5  $\mu\text{m}$  carbonate feature independently, without relying on the simultaneous presence of the 2.3  $\mu\text{m}$  band, which may not always be visible in sulfate-bearing regions. As carbonates and sulfates both require water to form and their abundance may help constrain past atmospheric conditions, properly identifying their complete extent and cooccurring minerals in orbital data is vital. These laboratory results provide new information that can aid both spectral modeling and orbital analysis that may help resolve a long-standing mismatch in orbital vs. *in situ* mineralogy of Mars.

## Data availability statement

The raw data supporting the conclusions of this article will be made available by the authors, without undue reservation.

## Author contributions

RS: Conceptualization, Funding acquisition, Investigation, Methodology, Project administration, Writing – original draft, Writing – review and editing. DL: Data curation, Investigation, Methodology, Software, Writing – original draft, Writing – review and editing. AF: Conceptualization, Writing – review and editing. ER: Conceptualization, Writing – review and editing. CP: Funding acquisition, Resources, Writing – review and editing. J-PB: Funding acquisition, Resources, Writing – review and editing.

## Funding

The author(s) declare that financial support was received for the research and/or publication of this article. A portion of this work was funded by the MSL Participating Scientist (80NSSC23K0189).

## Acknowledgments

We would like to thank the entire Mars Science Laboratory Team, especially the CheMin team, for collecting the mineralogical data that motivated this laboratory work. A portion of this research was carried out at the Jet Propulsion Laboratory, California Institute

## References

- Achilles, C. N., Rampe, E. B., Downs, R. T., Bristow, T. F., Ming, D. W., Morris, R. V., et al. (2020). Evidence for multiple diagenetic episodes in ancient fluvial-lacustrine sedimentary rocks in Gale Crater, Mars. *J. Geophys. Res. Planets* 125 (8), e2019JE006295. doi:10.1029/2019je006295
- Archer, P. D., Franz, H. B., Sutter, B., Arevalo, R. D., Jr., Coll, P., Eigenbrode, J. L., et al. (2014). Abundances and implications of volatile-bearing species from evolved gas analysis of the Rocknest aeolian deposit, Gale Crater, Mars. *J. Geophys. Res.* 119, 237–254. doi:10.1002/2013je004493
- Bandfield, J. L., Hamilton, V. E., and Christensen, P. R. (2003). A global view of Martian surface compositions from MGS-TES. *Science* 301 (5636), 1084–1087.
- Banin, A., Kan, I., and Margulies, L. (2007). Acidic volatiles and the Mars soil. *J. Geophys. Res. Planets* 112 (E5).
- Bell, J. F. (1996). “Iron, sulfate, carbonate, and hydrated minerals on Mars,” in *Mineral spectroscopy: a tribute to roger*. Editors G. Burns, M. D. Dyar, C. McCammon, and M. W. Schaefer (Houston, Tex: Geochem. Soc.), 359–380.
- Berger, J. A., Schmidt, M. E., Gellert, R., Campbell, J. L., Desouza, E., Flemming, R. L., et al. (2016). A global Mars dust composition refined by the alpha-particle X-ray spectrometer in Gale Crater. *Geophys. Res. Lett.* 43, 67–75. doi:10.1002/2015gl066675
- Bibring, J.-P., and Erard, S. (2001). The Martian surface composition. *Space Sci. Rev.* 96, 293–316. doi:10.1023/a:1011909708806
- Bibring, J.-P., Hamm, V., Pilorget, C., Vago, J. L., and the MicrOmega Team (2017). The MicrOmega investigation onboard ExoMars. *Astrobiology* 17 (6-7), 621–626. doi:10.1089/ast.2016.1642
- Bibring, J.-P., Langevin, Y., Gendrin, A., Gondet, B., Poulet, F., Berthe, M., et al. (2005). Mars surface diversity as revealed by the OMEGA/Mars express observations. *Sci. Sci.* 307 (5715), 1576–1581. doi:10.1126/science.1108806
- Bibring, J.-P., Langevin, Y., Mustard, J. F., Poulet, F., Arvidson, R. E., Gendrin, A., et al. (2006). Global mineralogical and aqueous Mars history derived from OMEGA/Mars Express data. *Science* 312 (5772), 400–404. doi:10.1126/science.1122659
- Bishop, J. L., King, S. J., Lane, M. D., Brown, A. J., Sanchez Roman, M., Hiroi, T., et al. (2021). Spectral properties of anhydrous carbonates and nitrates. *Earth Space Sci.* 8, 10. doi:10.1029/2021ea001844
- Bishop, J. L., Lane, M. D., Dyar, M. D., and Brow, A. J. (2008). Reflectance and emission spectroscopy study of four groups of phyllosilicates: smectites, kaolinite-serpentines, chlorites and micas. *Clay Miner.* 43, 35–54. doi:10.1180/claymin.2008.043.1.03
- of Technology, under a contract with the National Aeronautics and Space Administration (80NM0018D0004).

## Conflict of interest

The authors declare that the research was conducted in the absence of any commercial or financial relationships that could be construed as a potential conflict of interest.

## Generative AI statement

The author(s) declare that no Generative AI was used in the creation of this manuscript.

## Publisher's note

All claims expressed in this article are solely those of the authors and do not necessarily represent those of their affiliated organizations, or those of the publisher, the editors and the reviewers. Any product that may be evaluated in this article, or claim that may be made by its manufacturer, is not guaranteed or endorsed by the publisher.

Bishop, J. L., Murchie, S. L., Pieters, C. M., and Zent, A. P. (2002). A model for formation of dust, soil, and rock coatings on Mars: physical and chemical processes on the Martian surface. *J. Geophys. Res.* 107 (E11), 5097. doi:10.1029/2001je001581

Bishop, J. L., Tirsch, D., Tornabene, L. L., Neukum, G., McEwen, A. S., McGuire, P. C., et al. (2013). Mineralogy and morphology of geologic units at Libya Montes, Mars: ancient aqueously derived outcrops, mafic flows, fluvial features, and impacts. *J. Geophys. Res.* 118, 487–513. doi:10.1029/2012je004151

Blake, D. F., Morris, R. V., Kocurek, G., Morrison, S. M., Downs, R. T., Bish, D., et al. (2013). Curiosity at Gale Crater, Mars: characterization and analysis of the rocknest sand shadow. *Science* 341, 1239505. doi:10.1126/science.1239505

Blake, D. F., Vaniman, D. T., Achilles, C. A., Anderson, R., Bish, D., Bristow, T., et al. (2012). Characterization and calibration of the CheMin mineralogical instrument on Mars science laboratory. *Space Sci. Rev.* 170, 341–399. doi:10.1007/s11214-012-9905-1

Borg, L. E., Connelly, J. N., Nyquist, L. E., Shih, C. Y., Wiesmann, H., and Reese, Y. (1999). The age of the carbonates in martian meteorite ALH84001. *Science* 286 (5437), 90–94. doi:10.1126/science.286.5437.90

Boynton, W. V., Ming, D. W., Kounaves, S. P., Young, S. M. M., Arvidson, R. E., Hecht, M. H., et al. (2009). Evidence for calcium carbonate at the Mars Phoenix landing site. *Science* 325, 61–64. doi:10.1126/science.1172768

Bramble, M. S., Mustard, J. F., and Salvatore, M. R. (2017). The geological history of northeast Syrtis major, Mars. *Icarus* 293, 66–93. doi:10.1016/j.icarus.2017.03.030

Bridges, J. C., Catling, D. C., Saxton, J. M., Swindle, T. D., Lyon, I. C., and Grady, M. M. (2001). Alteration assemblages in martian meteorites: implications for near-surface processes. *Space Sci. Rev.* 96 (1), 365–392. doi:10.1007/978-94-017-1035-0\_13

Bridges, J. C., and Grady, M. M. (2000). Evaporite mineral assemblages in the nakhlite (martian) meteorites. *Earth Planet. Sci. Lett.* 176 (3), 267–279. doi:10.1016/s0012-821x(00)00019-4

Bridges, J. C., Hicks, L. J., and Treiman, A. H. (2019). “Carbonates on Mars,” in *Volatiles in the martian crust*. Editors J. Filiberto, and S. P. Schwenzer (Elsevier), 89–118.

Bristow, T. F., Haberle, R. M., Blake, D. F., Des Marais, D. J., Eigenbrode, J. L., Fairén, A. G., et al. (2017). Low hesperian PCO<sub>2</sub> constrained from *in situ* mineralogical analysis at Gale Crater, Mars. *P. Natl. Acad. Sci.* 114 (9), 2166–2170. doi:10.1073/pnas.1616649114

Bultel, B., Quantin-Nataf, C., Andréani, M., Clénet, H., and Lozac'h, L. (2015). Deep alteration between hellas and Isidis basins. *Icarus* 260, 141–160. doi:10.1016/j.icarus.2015.06.037

- Burns, R. G. (1993). *Rates and mechanisms of chemical weathering of ferromagnesian silicate minerals*. *Geochimica et Cosmochimica Acta*, 57, 4555–457.
- Burns, R. G., and Fisher, D. S. (1990). Iron-sulfur mineralogy of Mars: magmatic evolution and chemical weathering products. *J. Geophys. Res.* 95, 14415–14421. doi:10.1029/jb095ib09p14415
- Carter, J., and Poulet, F. (2012). Orbital identification of clays and carbonates in Gusev crater. *Icarus* 219, 250–253. doi:10.1016/j.icarus.2012.02.024
- Catling, D. C. (1999). A chemical model for evaporites on early Mars: possible sedimentary tracers of the early climate and implications for exploration. *J. Geophys. Res. Planets* 104 (E4), 16453–16469. doi:10.1029/1998je001020
- Changela, Chatzitheodoridis, E., Antunes, A., Beaty, D., Bouw, K., Bridges, J. C., et al. (2021). Mars: new insights and unresolved questions. *Int. J. Astrobiol.* 20, 394–426. doi:10.1017/s1473550421000276
- Chevrier, V., Poulet, F., and Bibring, J.-P. (2007). Early geochemical environment of Mars as determined from thermodynamics of phyllosilicates. *Nature* 448 (7149), 60–63. doi:10.1038/nature05961
- Chipera, S. J., and Vaniman, D. T. (2007). Experimental stability of magnesium sulfate hydrates that may be present on Mars. *Geochimica Cosmochimica Acta* 71 (1), 241–250. doi:10.1016/j.gca.2006.07.044
- Chipera, S. J., Vaniman, D. T., Rampe, E. B., Bristow, T. F., Martínez, G., Tu, V. M., et al. (2023). Mineralogical investigation of Mg-sulfate at the Canaima drill site, Gale crater, Mars. *J. Geophys. Res. Planets* 128, e2023JE008041. doi:10.1029/2023je008041
- Chou, I.-M., Seal, R. R., and Wang, A. (2013). The stability of sulfate and hydrated sulfate minerals near ambient conditions and their significance in environmental and planetary sciences. *J. Asian Earth Sci.* 62, 734–758. doi:10.1016/j.jseaes.2012.11.027
- Clark, J. V., Sutter, B., McAdam, A., Archer, P. D., Lewis, J., Franz, H., et al. (2024). “Changes in volatile mineralogy from the marker band valley to the layered sulfate-bearing unit in Gale Crater, Mars: results from the sample analysis at mars-evolved gas analyzer instrument,” in 55th Lunar and Planetary Science Conference, The Woodlands, United States (LPI Contribution).
- Clark, R. N., and Roush, T. L. (1984). Reflectance spectroscopy: quantitative analysis techniques for remote sensing applications. *J. Geophys. Res.* 89 (7), 6329–6340. doi:10.1029/jb089ib07p06329
- Clark, R. N., Swayze, G. A., Singer, R. B., and Pollack, J. B. (1990). High-resolution reflectance spectra of Mars in the 2.3  $\mu\text{m}$  region: evidence for the mineral scapolite. *J. Geophys. Res.* 95, 14463–14480. doi:10.1029/jb095ib09p14463
- Cloutis, E. A., Hawthorne, F. C., Mertzman, S. A., Krenn, K., Craig, M. A., Marcino, D., et al. (2006). Detection and discrimination of sulfate minerals using reflectance spectroscopy. *Icarus* 184 (1), 121–157. doi:10.1016/j.icarus.2006.04.003
- Dhondiyal, S., Porwal, A., Niveditha, C. V., Thangjam, G., Aranha, M., Kumar, S., et al. (2023). A novel algorithm for mapping carbonates using CRISM hyperspectral data. *Icarus* 397, 115504. doi:10.1016/j.icarus.2023.115504
- Drever, J. I. (1997). *The geochemistry of natural waters: surface and groundwater environments*. 3rd Edition. New Jersey: Prentice Hall.
- Edwards, C. S., and Ehlmann, B. L. (2015). Carbon sequestration on Mars. *Geology* 43 (10), 863–866. doi:10.1130/g36983.1
- Ehlmann, B. L., Mustard, J. F., Murchie, S. L., Bibring, J.-P., Meunier, A., Fraeman, A. A., et al. (2011). Subsurface water and clay mineral formation during the early history of Mars. *Nature* 479, 53–60. doi:10.1038/nature10582
- Ehlmann, B. L., Mustard, J. F., Murchie, S. L., Poulet, F., Bishop, J. L., Brown, A. J., et al. (2008). Orbital identification of carbonate-bearing rocks on Mars. *Science* 322 (5909), 1828–1832. doi:10.1126/science.1164759
- Ehlmann, B. L., Mustard, J. F., Swayze, G. A., Clark, R. N., Bishop, J. L., Poulet, F., et al. (2009). Identification of hydrated silicate minerals on Mars using MRO-CRISM: geologic context near Nili Fossae and implications for aqueous alteration. *JGR Planets* 114, E00D08. doi:10.1029/2009JE003339
- Fairén, A. B., Fernandez-Remolar, D., Dohn, J. M., Baker, V. R., and Amils, R. (2004). Inhibition of carbonate synthesis in acidic oceans on early Mars. *Nature* 431, 423–426. doi:10.1038/nature02911
- Gaffey, M. J. (1976). Spectral reflectance characteristics of the meteorite classes. *J. Geophys. Res.* 81 (5), 905–920. doi:10.1029/jb081i005p0905
- Gaffey, M. J. (1986). Reflectance spectroscopy of carbonate minerals in the visible and near-infrared (0.35–2.55 microns): applications in carbonate petrology. *J. Geophys. Res.* 91 (B13), 14033–14044.
- Gendrin, A., Mangold, N., Bibring, J.-P., Langevin, Y., Gondet, B., Poulet, F., et al. (2005). Sulfates in martian layered terrains: the OMEGA/Mars express view. *Science* 307, 1587–1591. doi:10.1126/science.1109087
- Góbi, S., and Kereszturi, A. (2019). Analyzing the role of interfacial water on sulfate formation on present Mars. *Icarus* 322, 135–143. doi:10.1016/j.icarus.2019.01.005
- Gooding, J. L., Arvidson, R. E., and Zolotov, M. Y. (1992). “Physical and chemical weathering,” in *Mars*. Editors H. H. Kieffer, B. M. Jakosky, C. W. Snyder, and M. S. Matthews (Tucson: Univ. Arizona Press), 626–651.
- Goudge, T. A., Milliken, R. E., Head, J. W., Mustard, J. F., and Fassett, C. I. (2017). Sedimentological evidence for a deltaic origin of the western fan deposit in Jezero crater, Mars and implications for future exploration. *Earth Planet. Sci. Lett.* 458, 357–365. doi:10.1016/j.epsl.2016.10.056
- Gyollai, I., Kereszturi, A., and Chatzitheodoridis, E. (2019). Analysis of shock metamorphic processes in the Zagami meteorite. *Cent. Eur. Geol.* 62, 56–82. doi:10.1556/24.61.2018.12
- Horgan, B. H., Anderson, R. B., Dromart, G., Amador, E. S., and Rice, M. S. (2020). The mineral diversity of Jezero crater: evidence for possible lacustrine carbonates on Mars. *Icarus* 339, 113526. doi:10.1016/j.icarus.2019.113526
- Hughes, E. B., Gilmore, M. S., Martin, P. E., and Eleazer, M. (2023). Visible to near-infrared reflectance and Raman spectra of evaporites from sulfate-chloride Mars analogue brines. *Icarus* 401, 115597. doi:10.1016/j.icarus.2023.115597
- Hunt, G. R., and Salisbury, J. W. (1970). Visible and near-infrared spectra of minerals and rocks—I. Silicate minerals. *Mod. Geol.* 1, 283.
- Hurowitz, J. A., McLennan, S. M., Tosca, N. J., Arvidson, R. E., Michalski, J. R., Ming, D. W., et al. (2006). *In situ* and experimental evidence for acidic weathering of rocks and soils on Mars. *J. Geophys. Res. Planets* 111 (E2), E02S19. doi:10.1029/2005je002515
- Kereszturi, A., Bradak, B., Chatzitheodoridis, E., and Ujvari, G. (2016). Indicators and methods to understand past environments from ExoMars rover drills. *Orig. Life Evol. Biospheres* 46, 435–454. doi:10.1007/s11084-016-9492-3
- Kijatani, Koike, M., Nakada, R., Tanabe, G., Usui, T., Matsuura, F., et al. (2023). Identification of carbonate-associated sulfate (CAS) in a noachian martian meteorite allan hills 84001. *Earth Planet. Sci. Lett.* 620, 118345. doi:10.1016/j.epsl.2023.118345
- King, P. L., Lescinsky, D. T., and Nesbitt, H. W. (2004). The composition and evolution of primordial solutions on Mars, with application to other planetary bodies. *Geochim. Cosmochim. Acta*, 68, 4993–5008. doi:10.1016/j.gca.2004.05.036
- King, P. L., and McSween, H. Y. (2005). Effects of H<sub>2</sub>O, pH, and oxidation state on the stability of Fe minerals on Mars. *J. Geophys. Res. Planets* 110 (E12), E12S10. doi:10.1029/2005je002482
- Kronyak, R. E., Kah, L. C., Edgett, K. S., VanBommel, S. J., Thompson, L. M., Wiens, R. C., et al. (2019). Mineral-filled fractures as indicators of multigenerational fluid flow in the Pahrump Hills member of the Murray formation, Gale crater, Mars. *Earth Space Sci.* 6 (2), 238–265. doi:10.1029/2018ea000482
- Leshin, L. A., Mahaffy, P. R., Webster, C. R., Cabane, M., Coll, P., Conrad, P. G., et al. (2013). Volatile, isotope, and organic analysis of martian fines with the Mars Curiosity rover. *Science* 341, 1238937. doi:10.1126/science.1238937
- Loizeau, D., Lequertier, G., Poulet, F., Hamm, V., Pilorget, C., Meslier-Lourit, L., et al. (2020). Planetary Terrestrial Analogues Library project: 2. building a laboratory facility for MicrOmega characterization. *Planet. Space Sci.* 193, 105087. doi:10.1016/j.pss.2020.105087
- Mandon, L., Parkes Bowen, A., Quantin-Nataf, C., Bridges, J. C., Carter, J., Pan, L., et al. (2021). Morphological and spectral diversity of the clay-bearing unit at the ExoMars landing site Oxia Planum. *Astrobiology* 21, 464–480. doi:10.1089/ast.2020.2292
- Mangold, N., Gendrin, A., Gondet, B., LeMouelic, S., Quantin, C., Ansan, V., et al. (2008). Spectral and geological study of the sulfate-rich region of west candor chasma, Mars. *Icarus* 194, 519–543. doi:10.1016/j.icarus.2007.10.021
- Martin, P. E., Farley, K. A., Baker, M. B., Malespin, C. A., Schwenzer, S. P., Cohen, B. A., et al. (2017). A two-step K-Ar experiment on Mars: dating the diagenetic formation of jarosite from Amazonian ground-waters. *J. Geophys. Res. Planets* 122, 2803–2818. doi:10.1002/2017je005445
- McSween, H. Y., Jr. (1994). What we have learned about Mars from SNC meteorites. *Meteoritics* 29, 757–779. doi:10.1111/j.1945-5100.1994.tb01092.x
- Michalski, J. R., and Niles, P. B. (2010). Deep crustal carbonate rocks exposed by meteor impact on Mars. *Nat. Geosci.* 3 (11), 751–755. doi:10.1038/ngeo971
- Milliken, R. E., Fischer, W. W., and Hurowitz, J. A. (2009). Missing salts on early Mars. *Geophys. Res. Lett.* 36 (11), L11202. doi:10.1029/2009gl038558
- Ming, D. W., Archer, P. D., Jr., Glavin, D. P., Eigenbrode, J. L., Franz, H. B., Sutter, B., et al. (2014). Volatile and organic compositions of sedimentary rocks in yellowknife bay, Gale Crater, Mars. *Science* 343, 1245267. doi:10.1126/science.1245267
- Mittelfeldt, D. W. (1994). ALH84001: a cumulate orthopyroxenite member of the Martian meteorite clan. *Meteoritics* 29, 900–221. doi:10.1111/j.1945-5100.1994.tb01106.x
- Morris, R. V., Ruff, S. W., Gellert, R., Ming, D. W., Arvidson, R. E., Clark, B. C., et al. (2010). Identification of carbonate-rich outcrops on Mars by the Spirit rover. *Science* 329, 421–424. doi:10.1126/science.1189667
- Morrison, S. M., Blake, D. F., Bristow, T. F., Castle, N., Chipera, S. J., Craig, P. I., et al. (2024). Expanded insights into martian mineralogy: updated analysis of Gale Crater’s mineral composition via CheMin crystal chemical investigations. *Minerals* 14, 773. doi:10.3390/min14080773
- Murchie, S., Arvidson, R., Bedini, P., Beisser, K., Bibring, J.-P., Bishop, J., et al. (2007). Compact Reconnaissance Imaging Spectrometer for Mars (CRISM) on Mars Reconnaissance Orbiter (MRO). *J. Geophys. Res.* 112, E05S03. doi:10.1029/2006JE002682

- Mustard, J. F., Ehlmann, B. L., Murchie, S. L., Poulet, F., Mangold, N., Head, J. W., et al. (2010). Composition, morphology, and stratigraphy of noachian crust around the Isidis basin. *J. Geophys. Res.* 114, E00D12. doi:10.1029/2009je003349
- Mustard, J. F., Murchie, S. L., Pelkey, S. M., Ehlmann, B. L., Milliken, R. E., Grant, J. A., et al. (2008). Hydrated silicate minerals on Mars observed by the Mars reconnaissance orbiter CRISM instrument. *Nature* 454, 305–309. doi:10.1038/nature07097
- Nachon, M., Mangold, N., Forni, O., Kah, L., Cousin, A., Wiens, R., et al. (2017). Chemistry of diagenetic features analyzed by ChemCam at pahrump hills, Gale Crater, Mars. *Icarus* 281, 121–136. doi:10.1016/j.icarus.2016.08.026
- Niles, P. B., Catling, D. C., Berger, G., Chassefière, E., Ehlmann, B. L., Michalski, J. R., et al. (2013). Geochemistry of carbonates on Mars: implications for climate history and nature of aqueous environments. *Space Sci. Rev.* 174, 301–328. doi:10.1007/s11214-012-9940-y
- O'Connor, J. T. (1968). Mineral stability at the Martian surface. *J. Geophys. Res.* 73, 5301–5311. doi:10.1029/jb073i016p05301
- Orofino, V., Goldspiel, J., Carofalo, I., Blanco, A., Fonti, S., and Marzo, G. (2009). Evaluation of carbonate abundance in putative martian paleolake basins. *Icarus* 200, 426–435. doi:10.1016/j.icarus.2008.11.020
- Phua, Y. Y., Ehlmann, B. L., Siljeström, S., Czaja, A. D., Beck, P., Connell, S., et al. (2024). Characterizing hydrated sulfates and altered phases in Jezero Crater fan and floor geologic units with SHERLOC on Mars 2020. *J. Geophys. Res. Planets* 129, e2023JE008251. doi:10.1029/2023je008251
- Poulet, F., Gomez, C., Bibring, J.-P., Langevin, Y., Gondet, B., Pinet, P., et al. (2007). Martian surface mineralogy from Observatoire pour la Mine ralogie, l'Eau, les Glaces et l'Activite on board the Mars Express spacecraft (OMEGA/MEx): Global mineral maps. *JGR* 112, E08S02. doi:10.1029/2006JE002840
- Rampe, E. B., Bristow, T. F., Morris, R. V., Morrison, S. M., Achilles, C. N., Ming, D. W., et al. (2020). Mineralogy of vera rubin ridge from the Mars science laboratory CheMin instrument. *J. Geophys. Res. Planets* 125 (9), e2019JE006306. doi:10.1029/2019je006306
- Riu, L., Pilorget, C., Hamm, V., Bibring, J.-P., Lantz, C., Loizeau, D., et al. (2022). Calibration and performances of the MicrOmega instrument for the characterization of asteroid Ryugu returned samples. *Rev. Sci. Instrum.* 93 (5), 054503. doi:10.1063/1.50082456
- Rivera-Hernández, F., Sumner, D. Y., Mangold, N., Banham, S. G., Edgett, K. S., Fedo, C. M., et al. (2020). Grain size variations in the murray formation: stratigraphic evidence for changing depositional environments in Gale Crater, Mars. *J. Geophys. Res. Planets* 125, e2019JE006230. doi:10.1029/2019je006230
- Robertson, K., and Bish, D. (2013). Constraints on the distribution of CaSO<sub>4</sub>NH<sub>2</sub>O phases on Mars and implications for their contribution to the hydrological cycle. *Icarus* 223, 407–417. doi:10.1016/j.icarus.2012.10.028
- Robertson, K. M., Milliken, R. E., and Li, S. (2016). Estimating mineral abundances of clay and gypsum mixtures using radiative transfer models applied to visible-near infrared reflectance spectra. *Icarus* 277, 171–186. doi:10.1016/j.icarus.2016.04.034
- Sheppard, R. Y., Milliken, R. E., Parente, M., and Itoh, Y. (2020). Updated perspectives and hypotheses on the mineralogy of lower Mt. Sharp, Mars, as seen from orbit. *J. Geophys. Res. Planets* 126, e2020JE006372. doi:10.1029/2020je006372
- Sheppard, R. Y., Milliken, R. E., and Robertson, K. M. (2022). Presence of clay minerals can obscure spectral evidence of Mg sulfates: implications for orbital observations of Mars. *Icarus* 383, 115083. doi:10.1016/j.icarus.2022.115083
- Sheppard, R. Y., Thorpe, M. T., Fraeman, A. A., Fox, V. K., and Milliken, R. E. (2021). Merging perspectives on secondary minerals on Mars: a review of ancient water-rock interactions in Gale crater inferred from orbital and *in-situ* observations. *Minerals* 11, 986. doi:10.3390/min11090986
- Siljeström, S., Czaja, A. D., Corpolongo, A., Berger, E. L., Li, A. Y., Cardarelli, E., et al. (2024). Evidence of sulfate-rich fluid alteration in Jezero Crater floor, Mars. *J. Geophys. Res. Planets* 129 (1), e2023JE007989. doi:10.1029/2023je007989
- Squyres, S. W., and Kasting, J. F. (1994). Early Mars: how warm and how wet? *Science* 265, 744–749. doi:10.1126/science.265.5173.744
- Stack, K. M., and Milliken, R. E. (2015). Modeling near-infrared reflectance spectra of clay and sulfate mixtures and implications for Mars. *Icarus* 250, 332–356. doi:10.1016/j.icarus.2014.12.009
- Stack, K. M., Williams, N. R., Calef, F., Sun, V. Z., Williford, K. H., Farley, K. A., et al. (2020). Photogeologic map of the Perseverance rover field site in Jezero crater constructed by the Mars 2020 Science Team. *Space Sci. Rev.* 216, 127. doi:10.1007/s11214-020-00739-x
- Stepcenkov, S., Wilhelm, T., and Woehler, C. (2022). Learning the link between albedo and reflectance: machine learning-based prediction of hyperspectral bands from CTX images. *Remote Sens.* 14, 3457. doi:10.3390/rs14143457
- Sun, V. Z., and Milliken, R. E. (2015). Ancient and recent clay formation on Mars as revealed from a global survey of hydrous minerals in crater central peaks. *J. Geophys. Res. Planets* 120, 2293–2332. doi:10.1002/2015je004918
- Sun, V. Z., Stack, K. M., Kah, L. C., Thompson, L., Fischer, W., Williams, A. J., et al. (2019). Late-stage diagenetic concretions in the Murray formation, Gale crater, Mars. *Icarus* 321, 866–890. doi:10.1016/j.icarus.2018.12.030
- Sutter, B., Boynton, W., Ming, D., Niles, P., Morris, R., Golden, D., et al. (2012). The detection of carbonate in the martian soil at the Phoenix landing site: a laboratory investigation and comparison with the Thermal and Evolved Gas Analyzer (TEGA) data. *Icarus* 218, 290–296. doi:10.1016/j.icarus.2011.12.002
- Sutter, B., Dalton, J. B., Ewing, S. A., Amundson, R., and McKay, C. P. (2007). Terrestrial analogs for interpretation of infrared spectra from the Martian surface and subsurface: sulfate, nitrate, carbonate, and phyllosilicate-bearing Atacama Desert soils. *J. Geophys. Res.* 112, G04S10. doi:10.1029/2006jg000313
- Sutter, B., McAdam, A. C., Mahaffy, P. R., Ming, D. W., Edgett, K. S., Rampe, E. B., et al. (2017). Evolved gas analyses of sedimentary rocks and eolian sediment in Gale Crater, Mars: results of the Curiosity rover's sample analysis at Mars instrument from Yellowknife Bay to the Namib Dune. *J. Geophys. Res. Planets* 122, 2574–2609. doi:10.1002/2016je005225
- Swindle, T. D., Treiman, A. H., Lindstrom, D. J., Burkland, M. K., Cohen, B. A., Grier, J. A., et al. (2000). Noble gases in iddingsite from the Lafayette meteorite: evidence for liquid water on Mars in the last few hundred million years. *Meteorit. Planet. Sci.* 35, 107–115. doi:10.1111/j.1945-5100.2000.tb01978.x
- Thorpe, M. T., Bristow, T. F., Rampe, E. B., Tosca, N. J., Grotzinger, J. P., Bennett, K. A., et al. (2022). Mars Science Laboratory CheMin data from the Glen Torridon region and the significance of lake-groundwater interactions in interpreting mineralogy and sedimentary history. *J. Geophys. Res. Planets* 127, e2021JE007099. doi:10.1029/2021je007099
- Tosca, N. J., Ahmed, I. A. M., Tutolo, B. M., Ashpittel, A., and Hurowitz, J. A. (2018). Magnetite authigenesis and the warming of early Mars. *Nat. Geosci.* 11, 635–639. doi:10.1038/s41561-018-0203-8
- Tutolo, B. M., Hausrath, E. M., Kite, E. S., Rampe, E. B., Bristow, T. F., Downs, R. T., et al. (2025). Carbonates identified by the Curiosity rover indicate a carbon cycle operated on ancient Mars. Science: Press.
- Vaniman, D. T., Bish, D. L., Chipera, S. J., Fialips, C. I., William Carey, J., and Feldman, W. C. (2004). Magnesium sulphate salts and the history of water on Mars. *Nature* 431, 663–665. doi:10.1038/nature02973
- Viviano-Beck, C. E., Seelos, F. P., Murchie, S. L., Kahn, E. G., Seelos, K. D., Taylor, H. W., et al. (2014). Revised CRISM spectral parameters and summary products based on the currently detected mineral diversity on Mars. *J. Geophys. Res. Planets* 119, 1403–1431. doi:10.1002/2014je004627
- Wang, A., Freeman, J. J., Chou, I.-M., and Jolliff, B. L. (2011). Stability of Mg-sulfates at –10°C and the rates of dehydration/rehydration processes under conditions relevant to Mars. *J. Geophys. Res.* 116, E12006. doi:10.1029/2011je003818
- Wang, A., Freeman, J. J., and Jolliff, B. L. (2009). Phase transition pathways of the hydrates of magnesium sulfate in the temperature range 50°C to 5°C: implication for sulfates on Mars. *J. Geophys. Res.* 114 (E4), E04010. doi:10.1029/2008je003266
- Wray, J. J., Murchie, S. L., Ehlmann, B. L., Milliken, R. E., Seelos, K. D., Noe Dobrea, E. Z., et al. (2011). Evidence for regional deeply buried carbonate-bearing rocks on Mars. *Lunar Planet. Sci.* 42, 2635.
- Wray, J. J., Murchie, S. L., Bishop, J. L., Ehlmann, B. L., Milliken, R. E., Wilhelm, M. B., et al. (2016). Orbital evidence for more widespread carbonate-bearing rocks on Mars. *J. Geophys. Res. Planets* 121 (4), 652–677. doi:10.1002/2015je004972
- Ye, C., and Glotch, T. D. (2019). Spectral properties of chloride salt-bearing assemblages: implications for detection limits of minor phases in chloride-bearing deposits on Mars. *J. Geophys. Res. Planets* 124, 209–222. doi:10.1029/2018je005859
- Yen, A. S., Ming, D. W., Vaniman, D. T., Gellert, R., Blake, D. F., Morris, R. V., et al. (2017). Multiple stages of aqueous alteration along fractures in mudstone and sandstone strata in Gale Crater, Mars. *Earth Planet. Sci. Lett.* 471, 186–198. doi:10.1016/j.epsl.2017.04.033
- Yoshida, N., Nakagawa, H., Terada, N., Evans, J. S., Schneider, N. M., Jain, S. K., et al. (2020). Seasonal and latitudinal variations of dayside N<sub>2</sub>/CO<sub>2</sub> ratio in the Martian thermosphere derived from MAVEN IUVS observations. *J. Geophys. Res. Planets* 125, e2020JE006378. doi:10.1029/2020JE006378